How does the rate of environmental change affect density-dependent population dynamics?

Christophe F. D. Coste[1,4], Brett Petersen[1], Dongbo Li[2], Chenggui Yuan[3], Steven M. Sait[2], and Mike S. Fowler[1,*]

[1]Department of Biosciences and Centre for BioMathematics, Swansea University, Singleton Park, SA2 8PP, UK
[2]School of Biology, University of Leeds, Leeds, LS2 9JT, UK.
[3]Department of Mathematics and Centre for BioMathematics, Swansea University, Bay Campus, SA1 8EN, UK.
[4]Department of Terrestrial Ecology, Norwegian Institute for Nature Research (NINA), Trondheim, Norway

Running title: Populations under environmental trends

Journal: Ecological Monographs

Type of article: Article

* **Corresponding author:**
Mike S. Fowler
E-mail: m.s.fowler@swansea.ac.uk ; Telephone: 01792 295 443
Department of Biosciences, Swansea University, Singleton Park, SA2 8PP, UK

E-mail addresses and ORCID:
Christophe F. D. Coste: c.f.d.coste.ecology@gmail.com and christophe.coste@nina.no, 0000-0003-3680-5049.
Brett Petersen: Brett.petersen@btinternet.com.
Dongbo Li: D.b.li@leeds.ac.uk, 0000-0003-0471-7917.
Chenggui Yuan: c.yuan@swansea.ac.uk, 0000-0003-0486-5450.
Steven M. Sait: S.M.Sait@leeds.ac.uk, 0000-0002-7208-8617.
Mike S. Fowler: m.s.fowler@swansea.ac.uk, 0000-0003-1544-0407.

Open research statement: No new data are used.

Keywords: tipping points; long transients; density-dependence; environmental trend; time of emergence; b-tipping points; r-tipping points; superimposition diagram; r-bifurcation diagram.

Content:
Number of words in the abstract: 224
Number of pages in the manuscript (main text): 64
The main text contains 1 text box and 13 figures .
The supplementary information (Appendix S1) contains 6 sections.

Abstract

Natural populations experience variable environments. Anthropogenically driven environmental change, in particular, is expected to impose trends on key demographic parameters such as reproduction and survival. Theoretical studies of how such environmental changes affect populations have highlighted dynamical phenomena including bifurcation-related tipping points – typically identified by comparing different, but constant, environmental states – and long transients – that can arise after sudden environmental perturbations. However, real-world environmental trends are neither instantaneous nor slow enough to justify treating the environment as constant, motivating recent interest in r-tipping points – regime shifts induced by r, the rate of environmental change in demographic parameters. Most existing work examines this phenomenon in complex ecological models and for specific values of r. Here, we develop tools to help ecologists investigate how populations and communities respond to environmental trends across a continuum of r values. Using a simple density-dependent model, we identify four qualitatively distinct responses to a trend as a function of r – patterns that traditional methods fail to reveal – and we visualize them using an *r-bifurcation diagram* introduced here. We also describe and mathematically explain the emergence of abrupt regime shifts linked to delayed bifurcations, revealed by a novel *superimposition diagram*. These findings are robust across modelling frameworks and ecological contexts, providing new insights into interactions between short- and long-term environmental change processes.

1 Introduction

The environment of natural populations varies over time and space, leading to changes in individual demographic parameters (reproduction, survival, dispersal, etc.) that, in turn, affect population abundances. These *time-varying demographic parameters* (the demographic rates varying with the environment, see glossary box 1) are often considered stationary (i.e., varying around a constant mean, see, e.g., Chevin et al., 2017; Saether et al., 2013; Lee et al., 2020). They may cycle regularly at different short-term, within-generation, timescales (e.g., diurnal, seasonal) and are subject to *environmental stochasticity* (random, short-term changes in the environment), but the mean demographic rate at the timescale of a relatively small number of generations is considered approximately constant (see, e.g., Nisbet and Gurney, 1985; Greenman and Benton, 2003).

Studies of the consequences of these environmental fluctuations on population dynamics have allowed ecologists to better understand the impacts of environmental stochasticity on population or community dynamics (Ruokolainen et al., 2009; Gilljam et al., 2019; Shoemaker et al., 2020; Ives and Carpenter, 2007). However, as a result of long-term climate change, the environment of natural populations is, in general, not stationary. Over timescales spanning multiple generations, the mean of many environmental signals that drive population dynamics follow a long-term trend, and therefore, do do environmentally-driven demographic parameters (Burke et al., 2018; Lear et al., 2020; Kemp et al., 2015; Song et al., 2021). These *environmental trends* can vary in both magnitude and rate of change.

Despite their increasing importance, as we face unprecedented, anthropogenically driven, climate change affecting temperatures (Hansen et al., 2006), precipitation (Le Treut and Somerville, 2007), and other key environmental drivers of populations (Gilljam et al., 2019; Cohen et al., 2018), we lack a comprehensive theoretical framework to examine how these environmental trends translate into quantitative and qualitative changes in population dynamics. This limits our

understanding of major global challenges, including the (in)variance of abundance fluctuations, future pest and disease outbreaks, threats from invasive species, and extinction risks. We require a new perspective on the general consequences of environmental trends on ecological populations, along with tools allowing us to better predict how focal populations or communities will fare during environmental trends, as a function of the realised rate of environmental change.

Long term environmental trends are expected to be accompanied by an increase in the variability of climate-change drivers (van der Wiel and Bintanja, 2021; Olonscheck et al., 2021). For example, the mean temperature of most habitats is expected to increase, along with the fluctuations around this mean (Lawson et al., 2015). Consequently, ecologists are now exploring the combined effects of these two aspects of global change, changing mean and increasing variance of demographic rates, on population dynamics (e.g., Campbell et al., 2012; Lawson et al., 2015). However, most studies focus solely on the direction and long-term magnitude of changes in the mean of time-varying demographic parameters, in a 'step-change' design that overlooks the rate at which these changes occur (see, e.g., Johnson et al., 2023; Burc et al., 2025; Van De Pol et al., 2010; Sæther et al., 2000; Kiritani, 2013). Using this "constant environment framework", compares population dynamics under two different, but constant, environmental regimes: a current and a projected future scenario. This framework neglects the population's trajectory between the old and new state, overlooking the potentially long transitional period between the initial and final environmental conditions. This approach ignores the "environmental debt" – the delayed effect of an environmental trend on population abundances – and generalises the concept of *extinction debt*, the delay in extinction encountered in deteriorating environments (Zarada and Drake, 2017; Highland and Jones, 2014; Ovaskainen and Hanski, 2002; Drake and Griffen, 2010). For a population undergoing an environmental trend, the journey towards the post-trend state may be as important as the destination.

Density-dependent populations, tipping points and long transients Many dynamic population or community models incorporate some dependence of demographic rates on population abundances (Krebs, 1995; Elton and Nicholson, 1942; Royama, 1992). Density dependence can yield qualitatively distinct population dynamics in constant environments, such as stable point equilibria (including extinction), cycles and chaos, both in models and in natural populations (May, 1974, 1976; Brauer and Castillo-Chavez, 2013; Barraquand et al., 2017; Myers, 2018; Mitani and Mougi, 2017; Rogers et al., 2022). The same species can exhibit qualitatively different dynamics in different environments; e.g., *Microtus* and *Clethrionomys* voles display quasi-stationary dynamics in the southern part of Fennoscandia and large amplitude quasi-cycles in the northern part (Korpimäki et al., 2005; Graham and Lambin, 2002; Turchin and Ellner, 2000). The responses of density-dependent populations to (abiotic) environmental changes has prompted the recent development of the *tipping-point* and *long-transient* frameworks in population biology (Hastings et al., 2018; Morozov et al., 2020; Francis et al., 2021; Abbott et al., 2024).

Bifurcation diagrams illustrate the long-term, steady-state (asymptotic) population dynamics as a function of certain environmentally-driven demographic parameters (Fig.1). At certain parameter values, called *bifurcations*, the asymptotic behaviour changes qualitatively. Assuming that a very slow environmental trend produces dynamics predicted by the constant environment framework, population abundances are expected to encounter a *regime shift* (a qualitative change of the dynamics, Hastings et al., 2018) as a parameter passes, very slowly, through a bifurcation point.

For discontinuous (or critical) bifurcations, which correspond to abrupt changes in abundances where there is no (positive) equilibrium point on one side of the bifurcation (such as fold or saddle-node bifurcations, see, e.g., Boettiger and Batt, 2020), this leads to *tipping points* – sudden, quantitative changes in the dynamics (also called *b-tipping points* as they are related to bifurcations, Scheffer et al., 2001; Dakos et al., 2012; Boettiger and Hastings, 2012). A system may not recover from passing a tipping-point (even when returning to previous conditions, because of hysteresis, Scheffer et al., 2001b) and the approach to the bifurcation may exhibit a

critical slow down (increasingly slow recovery from perturbations, Scheffer et al., 2009). Continuous (e.g., period doubling) bifurcations, do not show drastic abundance changes, and are deemed more innocuous than their discontinuous counterparts, therefore have received less attention. For both types of bifurcations, however, we still largely ignore how slow an environmental trend must be to ensure the dynamics correspond to predictions from the constant environment framework, or how fast before this assumption breaks down (Vanselow et al., 2019).

An alternative simplifying assumption is that the consequences of an environmental trend can be approximated by considering it instantaneous (a step-change), related to the study of *long transients*. A transient is the route a dynamical system takes following a perturbation to conditions, before reaching the long-term state of the system under the new conditions (Levin, 1976). This transient phase can be relatively short. However, even in simple population models, the time required to reach the asymptotic state can be significantly longer than the species' generation time, e.g., 20-30 generations in the prey-predator model of Poggiale (2020), or up to "hundreds of generation times" in the age-structured single population model of Morozov et al. (2016). Transitional periods of up to 100 generations have been observed in empirical systems and interpreted as *long transients* (Hastings et al., 2018). The study of *long transients* therefore provides an alternative framework for investigating dynamical regime shifts.

Morozov et al. (2016) showed that both the duration of the transient regime and the final asymptotic regime are hard to predict when multiple attractors exist. Understanding transient dynamics is further complicated by the possibility of regime shifts *during* the transient period (Carpenter et al., 2011; Boettiger and Hastings, 2012), which can be caused, e.g., by "crawl-bys" (when abundances pass close to an unstable, saddle, equilibrium Hastings et al., 2018; Rubin et al., 2022). The study of long transients has highlighted the risk of focusing only on the constant environment framework, showing that, while the asymptotic dynamics indicate that populations are safe from quasi-extinction, populations can fall below that threshold during the transient period (Morozov et al., 2020, 2024). A realistic trend is neither an instantaneous change, nor so

slow that the environment can be considered constant. Recent studies of the effect of the *rate of change* of the time-varying demographic parameter itself (Williams et al., 2021), have revealed that it can induce tipping points (*r-tipping points*, Ashwin et al., 2012; Siteur et al., 2016).

Rate of environmental change, *r*-tipping points and population dynamics The existence, relevance and mechanisms of *r-tipping points* in ecological systems show that, in many cases, the rates of environmental change are at least as important as the magnitude of the change (Abbott et al., 2024; Ritchie et al., 2023; Vanselow et al., 2022, and references therein). *r-tipping points* are related to the idea of *environmental tracking* (i.e., how closely a population's abundance fluctuations follow environmental changes, Roughgarden, 1975), occurring when the environment changes too quickly for the population to track the environmental change (Abbott et al., 2024). E.g., rapid increases in fishing pressure in coral reef ecosystems are predicted to lead to system collapse, while slower increases of the same total magnitude result in persistence (Gil et al., 2020).

The unprecedented rate of change of many anthropogenically driven environmental factors are expected to impact ecosystems more than the magnitude of the change (Vitousek, 1994; Sage, 2020) and could (far) exceed the rate at which populations and communities can track these changes (Walther et al., 2002). These studies show that *r*-tipping points may exist in many systems with discontinuous bifurcations, raising the question of whether naturally observed regime shifts tend to be rate- or bifurcation-induced (Vanselow et al., 2019). They do not, however, consider the general effects of the rate of environmental change on population dynamics and, in particular, how this rate can affect populations as they pass by bifurcations, with the notable exception of the transcritical bifurcation (i.e., bifurcation to extinction Zarada and Drake, 2017). Extending the study of the consequences of the rate of environmental change (which we term r here) beyond *r*-tipping points and for any bifurcation, is, therefore, a key advance. This will allow ecologists to understand the range of r for which the constant environment or transient dynamics framework(s) are valid and, more generally, how populations will behave across a range of environmental trends.

Here, we address these knowledge gaps, focusing on the validity of these two simplifying assumptions, by analysing the consequences of the speed of an environmental trend r on population trajectories over time. We consider a continuum of r-values, and study the ways r affects the dynamics, such as r-tipping points, as well as more general effects of r on population time-series, demonstrating that even continuous bifurcations can lead to b-tipping points. We provide a novel tool to study the effect of non-stationary environmental changes on population dynamics – the *r-bifurcation diagram* – depicting the value(s) of the time-varying demographic parameter(s) corresponding to regime shifts, as a function of the rate of environmental change (r). We illustrate our analysis with a simple density-dependent model for an unstructured population that reproduces at discrete time intervals.

We initially explore an environment that impacts demographic rates, with a simple, linearly increasing trend, comparing our findings with predictions from constant environment and transient dynamics frameworks. We show that qualitative shifts in population dynamics driven by an environmental trend are delayed compared to the corresponding constant environment framework and can lead to b-tipping points, especially for fast trends. We illustrate this with *superimposition diagrams* which allow us to compare the bifurcation diagram with the abundance time-series, in a re-scaled timescale directly related to demographic rates. We analyse the mechanisms underpinning these results and introduce a novel categorisation of four rates of environmental change, ranging from *very slow* to *very fast*, as a function of their effect on b-tipping points and transient dynamics. We show that our main findings are general enough to apply in more complex ecological models, including those with stochastic fluctuations around the linear trend and in continuous-time, multi-species models.

2 A simple, deterministic density-dependent population model

In a constant environment, the population projection equation of the logistic map is (May, 1976):

$$n_{t+1} = f(n_t) = \lambda n_t(1 - n_t) \tag{1}$$

Here, n_t is the population abundance (scaled by the carrying capacity) at generation t and λ is the reproductive rate (i.e., the number of offspring produced by an adult before dying). Density-dependence arises through the $(1 - n_t)$ term, representing the proportion of offspring that survive the juvenile period as a (decreasing) function of n_t. We can predict the final, long-term (asymptotic) population densities (or *attractor*) that populations will approach from any *non-trivial* initial condition ($n_0 > 0$). When $\lambda < 1$, the population approaches a so-called *trivial* (extinction) equilibrium (i.e., $n_t \to 0$). For $1 < \lambda < 3$, this is a *stable point* equilibrium:

$$\hat{n}(\lambda) = 1 - \frac{1}{\lambda}. \tag{2}$$

The bifurcation diagram (Figure 1) shows that for $\lambda > 3$, $\hat{n}(\lambda)$ is no longer stable (i.e., $\hat{n}$ is a repeller, rather than an attractor; shown in grey). At $\lambda = 3$ (itself corresponding to a – neutrally – stable point equilibrium) a bifurcation occurs from a single-point equilibrium to a 2-generation cycle (i.e., the population fluctuates deterministically between two different abundances in alternate generations); this bifurcation is continuous (there is no discontinuity in the bifurcation diagram at $\lambda = 3$). Further increasing λ generates subsequent period-doubling bifurcations towards 4-, then 8-, then 16-generation cycles, etc., followed by the onset of chaos (at $\lambda \approx 3.54$). The chaotic range (interspersed with "periodic windows"; Appendix S1: Section A1) lasts until the maximum reproductive rate of $\lambda = 4$.

Predicting the consequences of environmental change from the constant environment framework, as is classically (and often implicitly) done in ecology, implies considering the asymptotic (long-term) abundance behaviour at two demographic parameter values (considered as two

distinct, constant environments). In other words, for a "slow" speed of environmental change, the abundances observed over time (n_t) are expected to correspond to the asymptotic abundances of the bifurcation diagram (Fig.1) and to follow a relatively simple trajectory between the corresponding starting and final regimes. No b-tipping point is predicted to occur as bifurcations are continuous (see Appendix S1: Section A2).

Transient dynamics of the logistic map

A bifurcation diagram describes the asymptotic population dynamics, but ignores the transient phase leading to this final dynamical state. For example, the bifurcation diagram of figure 1 does not distinguish between the under- and over-compensatory transient approaches to the equilibrium attractor around $\lambda = 2$ (which we have therefore differentiated with blue and magenta colours). This distinction is crucial for transient regimes, as well as when studying environments that fluctuate around a fixed mean value (Nisbet and Gurney, 1985; Greenman and Benton, 2003). The sign and the amplitude of the derivative of the population growth function f (eq.1) – i.e., the Jacobian, see Appendix S1: Section A1 – provides useful information for small deviations from the equilibrium and for certain equilibria, but is not generally sufficient to understand the road to the asymptotic behaviour. E.g., for very close initial population values (n_0), transients that approach the same asymptotic behaviour can take very different paths, with the transient period differing wildly in duration (Poggiale, 2020; Morozov et al., 2016; Hastings et al., 2018). This also holds for the logistic map: e.g., for $\lambda = 3.9605$, which corresponds to a 4-generation asymptotic cycle, the transient period can vary between 1 and 850 generations, depending on the value of n_0 (see Appendix S1: Section A1).

The Logistic map with an environmental trend

Here, we consider a case where the reproductive rate changes consistently over time (λ_t, eq.3a). To reduce the number of parameters, we first consider a simple, linear, environmental trend (eq.3b) – but relax this assumption in Appendix S1: Section A4, showing qualitatively similar

results – via the following system of equations:

$$\begin{cases} n_{t+1} = \lambda_t n_t (1 - n_t) & \text{(3a)} \\ \lambda_t = \lambda_0 + rt \text{ for } 0 \leq t \leq T \text{ and } \lambda_t = \lambda_T \text{ for } t \geq T \quad , & \text{(3b)} \\ \lambda_0 = 1.001 \text{ and } \lambda_T = 3.9605 & \text{(3c)} \\ n_0 = \hat{n}(\lambda_0) \approx 0.001 & \text{(3d)} \end{cases}$$

where T is the duration of the environmental trend and r the rate of environmental change (of the time-varying demographic parameter, here the reproductive rate). We initiate the population at a non-zero stable equilibrium (as $1 < \lambda_0 < 3$). It then encounters a novel trend in the environment that "benefits" the population by increasing the reproductive rate: λ_t increases over time, i.e., the rate of environmental change $r > 0$. We set the initial reproductive rate at $\lambda_0 = 1.001$ (eq.3c), which corresponds to $n_0 = \hat{n}(1.001) \approx 0.001$ (eq.3d and eq.2). However, we note that our main conclusions hold when we start with higher λ_0 values and consider a "negative" environmental trend that reduces reproductive output over time ($r < 0$, Appendix S1: Section A5). We focus primarily on understanding how population abundance n_t responds to the environmental trend, i.e., for $0 \leq t \leq T$.

However, we are also interested in how the environmental trend affects the post-trend dynamics, we, therefore, also consider the population dynamics after the environmental trend (n_t for $t \geq T$). For that part of the time-series, the environment is held constant at $\lambda_{t \geq T} = \lambda_T$, and the abundance time-series correspond to transient dynamics with initial condition n_T (see Appendix S1: Section A1). To identify the time at which the population stabilises near the asymptotic dynamics, we want λ_T to correspond to an asymptotic cycle of short period, while still being close to the maximum reproductive rate, $\lambda = 4$, so that the trend goes though as wide a range of λ values (corresponding to non-extinct populations) as possible. Therefore, we end the environmental trend at generation T, such that $\lambda_T = 3.9605$ (eq.3c), which produces an asymptotic 4-generation cycle (see Fig.1 and Appendix S1: Section A1). The environmental trend duration T and its speed

r are related: from eq.3, we have $r = \frac{\lambda_T - \lambda_0}{T} \approx \frac{2.96}{T}$. We study the dynamics of this population for various rates of environmental rates of change (r) in the following section, and go on to show that our key findings hold in more complex ecological frameworks.

3 Population dynamics under an environmental trend

3.1 A *slow* trend

We initially consider a trend that lasts for $T_s = 7,000$ generations (i.e., $r_s \approx 4.2 \times 10^{-4}$). This allows us to illustrate key dynamical features before introducing other rates of environmental change below. This trend can be considered slow by contrast to the internal pace of change of the system, which can yield transients of up to ≈ 850 generations (see Appendix S1: Section A1) and asymptotic cycles of less than 4 generations for most of the range of λ_t (Fig.1).

The time series of a population affected by this *slow* environmental trend (Figure 2a) initially appears to correspond to the constant environment bifurcation diagram (Fig.1): population abundances (blue) increase monotonically over time until they start oscillating (Figures 2b and 2c). We denote the generation at which these oscillations start as

$$t_o(r) = min_t\{t, n_{t+1} < n_t\}$$

For this *slow* trend, we have $t_o(r_s) = 5074$ (Fig. 2c). These oscillations are initially 2-generation quasi-cycles with mean and amplitude increasing over time, followed by quasi-cycles of period 4 and almost immediately by chaotic behaviour (at around $t = 6100$, $\lambda_t \approx 3.55$). Once the trend is over, at $t = T$, the abundances stabilise at the asymptotic 4-generation cycle associated with λ_T, here, following a post-trend transient of around 25-30 generations (indicated by the initial fluctuations after the vertical black line in Fig.2a). Surprisingly, as the period doubling bifurcations of the constant environment framework are continuous and therefore expected to

correspond to smooth regime shifts for *slow* trends, we observe that the transition from monotonically increasing abundances to oscillations (Fig.2a) leads to an abrupt increase in cycle amplitude, that occurs over ~ 60 generations starting at t_o (Fig.2b), before the increase in amplitude slows pace.

The *superimposition diagram*

To compare abundance dynamics for various rates of environmental change (r, and corresponding T), we turn to an alternative timescale: λ_t. Instead of counting time as the succession of generations, this timescale counts it as increments in the demographic parameter affected by the environment. This transformation is valid for the period of environmental change, $0 < t < T$, where λ_t is a strictly monotonic function of t: each value of λ_t (top axis on Fig.2) corresponds to a unique value of t. We can study directly the abundance trajectories in this alternative timescale via *function composition*, an operation that creates a new function by applying one function to the result of another (i.e., nesting functions). The function composition of $n_t = n(t)$ – in blue on Fig.2 – and $t(\lambda_t)$ – the inverse of $\lambda_t = \lambda(t)$, in red on Fig.2 – yields $n(\lambda_t) = n(t(\lambda_t))$ – in blue on Fig.3. This alternative timescale allows us to superimpose the abundance time-series onto the bifurcation diagram (in black on Fig.3).

This *superimposition diagram* shows the abundances initially tracking the *moving equilibrium* $\hat{n}_t$ (in red on Fig.3, see glossary box 1):

$$\hat{n}_t = \hat{n}(\lambda_t) = 1 - \frac{1}{\lambda_t} \tag{4}$$

Emergence of a b-tipping point

After passing the first period-doubling bifurcation of the constant environment framework, at $\lambda = 3$, the population continues to grow monotonically and track the moving equilibrium ($\hat{n}_t$) despite it being in a range corresponding to unstable point-equilibria (2-generation cycle) in the constant environment. In that range, the moving equilibrium is a *ghost attractor*, a

non-equilibrium state that would be an (unstable) equilibrium in a constant environment. Abundances (n_t) track the ghost attractor ($\hat{n}_t$) for some time, until a qualitative shift in dynamics occurs once the time-varying reproductive rate (λ_t) passes $b(r_s) = \lambda_{t_o} \approx 3.146$ (grey vertical line on Fig.2) when abundances start oscillating . The difference between this observed value and the constant-environment bifurcation (i.e., here, $b(r_s) - 3$) constitutes a *delay in the bifurcation*. This phenomenon has been studied by mathematicians (e.g., Baer et al., 1989; Tsuchiya and Yamagishi, 1997; Miyazaki and Tchizawa, 2005) but rarely in the context of environmental change, with the exception of the transcritical (extinction) bifurcation (at $\lambda = 1$, e.g., Zarada and Drake, 2017; Drake and Griffen, 2010). The subsequent abrupt and rapid increase in the amplitude of oscillations corresponds to the population abundances rapidly catching up with that of the 2-generation cycles of the constant environment framework (here the quasi-2-generation-cycles are reached at $\lambda \approx 3.174$, see Figures 2b and 3 (insert)), which constitute a new ghost equilibrium (of period 2).

We can quantify the abruptness of this quantitative shift (the increasing amplitude of oscillations) by considering, first, the rate of change of the population abundances s_t (the discrete time equivalent to the first derivative) and, second, the rate of change of this rate of change, the abundance *acceleration* a_t (the second derivative):

$$\begin{cases} s_t = |n_{t+1} - n_t| \\ a_t = |s_{t+1} - s_t| \end{cases} \tag{5}$$

Figure 4 shows the acceleration time series (a_t) for various rates of environmental change (r, slower than the *slow* trend, i.e., $r < r_s$). For each value of r, the acceleration is very small most of the time but for a peak (occurring shortly after $b(r)$) where it reaches a maximum acceleration, that we denote $d(r)$ (the peak value on Fig.4):

$$d(r) = \max_t(a_t) \tag{6}$$

This abrupt, qualitative and quantitative change, shifts the dynamical regime quickly from a monotonic increase in abundances to cycles of large amplitude: $b(r)$ is a b-tipping point (of size $d(r)$).

Both $b(r)$ and $d(r)$ increase with the rate of environmental change (r). The slower the trend, the closer the b-tipping point $b(r)$ is to $\lambda = 3$ and the maximum acceleration in abundances $d(r)$ is to 0 (see Fig.S5 of Appendix S1: Section A2; formally, $\lim_{r\to 0} b(r) = 3$ and $\lim_{r\to 0} d(r) = 0$). As a consequence, $b(r)$ is not a b-tipping point for a (paradoxical) trend of speed $r = 0$, but is one for any real trend ($r > 0$, see Appendix S1: Section A2). We focus here on this particular b-tipping-point, but note that the other period doubling bifurcations can also be delayed (see below and Appendix S1: Section A2). We provide a mechanistic and graphical explanation for this delay in bifurcation and related b-tipping point, via cobweb diagrams, in section 5.1, and a more detailed mathematical analysis of the abundance behaviour, via the concepts of repelling boundaries and cascading effects, in section 5.2.

3.2 Slower and Faster trends

We now consider a *very slow* (*vs*) environmental trend, where it takes $T_{vs} = 1 \times 10^8$ generations to reach λ_T from λ_0 (i.e., $r_{vs} \approx 3 \times 10^{-8}$). The corresponding superimposition diagram (Figure 5a) shows the realised abundance dynamics display closer alignment with the bifurcation diagram. However, the b-tipping point at $\lambda = b(r)$ exists for any non-zero trend (Fig.4), even a *very slow* one (Fig.5b, here, $b(r_{vs}) = 3.0009$). The delay in the bifurcation ($b(r_{vs}) - 3$) causes a sudden acceleration in the dynamics and a rapid increase in cycle amplitudes (Fig.5b), even though the amplitude of the discontinuity is smaller ($d(r_{vs}) < d(r_s)$, see Fig.4) and the delay shorter in the λ_t *timescale* than for the slow trend ($3 < b(r_{vs}) < b(r_s)$). Below, we show that, as the rate of environmental change r decreases, the delay in bifurcation actually increases on the *chronological* timescale: $t_o(r) - t_3(r)$, where $\lambda_{t_3} = 3$, is a decreasing function of r. Therefore, the slower the trend, the more generations it takes for the first oscillation to occur, after passing $\lambda = 3$ (and

$\lim_{r\to 0} t_o(r) - t_3(r) = +\infty$).

There are quantitative, but not qualitative differences in abundance dynamics between the *slow* and the *very slow* trends; e.g., changes in the b-tipping point, $b(r)$, in the generation of the onset of abundance oscillations, $t_o(r)$, and in the maximum acceleration in the amplitude of oscillations, $d(r)$. However, differences in the post-trend transient behaviour do justify distinguishing between *slow* and *very slow* environmental trends. Under the *very slow* environmental trend ($r = r_{vs}$), the population abundance at the end of the trend (n_T) is close enough to one of the four points of the 4-generation asymptotic cycle associated with $\lambda_T = 3.9605$, that there is no observable transient (Fig.5c). Under the *slow* trend ($r = r_s$), a post-trend transient of 20-30 generations can be observed (Fig.2a). For the *very slow* trend, there is a short delay (in the demographic time-scale) for both the first and the second bifurcation (from 2- to 4-generation cycles), while for the *slow* trend (Fig.3), the second delay is so long that pseudo 4-generation cycles do not occur. Despite the self-similarity of the logistic map (Tan and Chia, 1996), it is possible for a given rate of environmental change (r) to encounter a b-tipping point at one period-doubling bifurcation and not others.

The onset of cycling can be delayed further (on the demographic timescale, λ_t), with faster environmental trends. For a *fast* environmental trend spanning $T_f = 225$ generations ($r_f \approx 0.013$), the population grows monotonically during the entire trend and only starts oscillating once the trend is over; i.e., $b(r_f) = \lambda_T = 3.9605$ (Figure 6). At the beginning of the trajectory ($\lambda_0 = 1.001$, $n_0 = \hat{n}_0 = 0.001$), the abundances struggle to track the rapidly changing environment (compare blue and red lines around $\lambda_t = 1$ in Fig.6), but eventually recover, tracking the environment (i.e., the moving/ghost equilibrium $\hat{n}_t$) until the end of the trend ($t = T$). This lagged "dip" at the start of the abundance trajectory ($1 < \lambda_t \ll 2$) occurs for all trends, but is barely noticeable on the abundance time series for the *slow* trend (Figs 2 and 3) and not at all for the *very slow* trend (Fig.5). We provide a mathematical analysis of this phenomenon in section 5.2 and summarise the key dynamical differences of the three characteristic rates of environmental considered so far via

plots of abundance dynamics in chronological time, superimposition diagrams (demographic timescale, λ_t) and cobweb diagrams, in Appendix S1: Section A2.

The speed of the environmental trend can be increased up to $r_{vf} \approx 2.96$, corresponding to $T_{vf} = 1$ generation. Here, the trend corresponds to an instantaneous (step-) change (see Fig.S6d in Appendix S1: Section A2). Contrary to slower trends, there is no initial monotonic increase in abundances; the dynamics consist exclusively of a post-trend transient which lasts around 80 generations (from $n_0 = 0.001$), before settling on the asymptotic 4-generation cycle. The duration and behaviour of the transient is very sensitive to the choice of initial condition (n_0) and constant environment parameter (λ_T) (see Appendix S1: Section A1). We refer to environmental trends that lead to dynamics that are dominated by transients, as *very fast* trends; we will see that, for our study, they consist of the step-change ($T = 1$) and trends made of a small number of generations ($T < 34$) .

Because the transient of a step-change is very sensitive to the initial conditions, the duration and behaviour of the transient stemming from a trend of a few steps will be very sensitive to the number of steps taken to reach λ_T: for $T = 2$, the transient drops to 3 generations, yet for $T = 3$ it increases to 230 generations (see Appendix S1: Section A6). As a consequence, the generation of first oscillation t_o and its corresponding value of time-varying reproductive rate, $b(r) = \lambda_{t_o}$, are similarly unpredictable under *very fast* trends, which contrasts with the predictability of *fast* trends (where, e.g., $b(r_f) = \lambda_T = 3.9605$). To illustrate these points and better understand what is happening along this r-continuum, we introduce the *r-bifurcation diagram*.

3.3 The *r-bifurcation diagram*

We have considered four speeds of the environmental trend ($r = r_s, r_{vs}, r_f$ and r_{vf}) and the corresponding population dynamics. The metrics we developed, including the generation of the first abundance oscillation, $t_o(r)$ and the associated value of the reproductive rate $b(r) = \lambda_{t_o}$ (the b-tipping point), allow us to go further and compare abundance dynamics under a continuum of

environmental trends. Here we introduce another metric: the duration of the post-trend transient, $D(r)$ (Appendix S1: Section A1). Figure 7 introduces the *r-bifurcation diagram* which displays the b-tipping point $b(r)$ (blue points) and the duration of the post-trend transient $D(r)$ (red points) as a continuous function of the rate of environmental change (r). This diagram allows us to identify four qualitatively different rates of environmental change (r) – of which the four specific speeds of the environmental trend we have studied (*very slow*, *slow*, *fast* and *very fast*) are archetypes– and to characterise their range. We will use the same names for the general ranges of r corresponding to qualitatively different dynamics than for their archetypes studied above: .

The *r-bifurcation diagram* shows that the value of the time-varying demographic parameter (λ_t) at which oscillations start (the b-tipping point, $b(r)$), tends towards $b(0) = 3$ as the speed of environmental change slows towards $r = 0$ (Fig. 7). The r-bifurcation diagram further shows that $b(r)$ initially increases with the speed of the environmental trend (r) (*very slow* and *slow* environmental trends, Fig.4 and Fig. 7), but this initial increase plateaus at $b(r) = \lambda_T$ (the maximum possible value for λ_t) for a value of $r = r^\dagger \approx 0.0114$ (corresponding to $T = 259$ generations), which allows us to distinguish between *slow* and *fast* trends; across a range of environmental change values $r^\dagger < r < r^*$, all trends are characterised as *fast*: $b(r) = \lambda_T$. Very fast trends occur above $r^* \gtrapprox 0.0870$ ($T \leq 34$ generations), including the step-change ($T = 1$): they correspond to cases where $b(r)$ (that differs from λ_T) is a non-monotonic function of r. Figure 7 shows the b-tipping point ($b(r)$) initially decreasing rapidly, after r^*, to $b(r) \approx 2.5$, before returning to $b(r) \to \lambda_T = 3.9605$. For such rapid environmental trends, transient dynamics drive the abundance patterns, and render the duration and behaviour of transients unpredictable, so that, for some values of r, the onset of oscillations can occur before the end of the environmental trend, i.e., $b(r) < \lambda_T$ or even before the constant-environment bifurcation, i.e., $b(r) < 3$, (black dots in the *very fast* section of Fig.7).

Contrary to the continuous transition between *slow* and *fast* trends, and partly caused by the choice of λ_T (noting we are restricted to $\lambda_T < 4$ for this simple model), the *fast—very fast*

transition, r^*, induces a regime shift: it is an *r-tipping point*. On the fast side of r^*, population abundances grow monotonically during the entire duration of the trend; on the very fast side, they can start oscillating earlier. The $b(r)$ metric does not segregate between *very slow* and *slow* trends, but $D(t)$ – the duration of the post-trend transient – does: *very slow* trends correspond to $r < \check{r} \approx 5.7 \times 10^{-7}$, for which there is no post-trend transient: the environmental trend is slow enough, and therefore n_T close enough to the asymptotic cycle, that the abundances converge immediately on the cycle as the environmental trend ends.

We can perform the same analysis on the chronological timescale by considering the time at which the first population decline is observed, $t_o(r)$. That is, the number of generations for which the abundance keeps increasing monotonically having passed the constant environment bifurcation point $\lambda_{t_3} = 3$, i.e., $t_o - t_3$ (Fig.S8 in SMA2). The slower the environmental trend (r), the more generations the population monotonically increases, after having passed $\lambda = 3$, and the (chronological) delay in oscillation ($t_o(r) - t_3(r)$) tends towards ∞ as r tends towards 0.

In summary, by considering dynamics on chronological and demographic (λ_t) timescales, we have identified that, for a given (even simple, continuous) bifurcation (here, at $\lambda = 3$), environmental trends can generate *b-tipping points* and be categorised into four categories (see Figure 8):

- *Very slow* trends show a delayed bifurcation/b-tipping point (corresponding, for the logistic map, to $3 < b(r) \ll \lambda_T$), but do not show post-trend transients at $\lambda_{t \geq T}$.
- *Slow* trends also show a delay in the bifurcation, after which abundances start cycling, with transients at the end of the trend.
- For *fast* trends, the bifurcation delay extends to the end of the trend. Before then, abundances follow the moving/ghost equilibrium (here, $b(r) = \lambda_T$; abundances grow monotonically until the end of the trend).
- *Very fast* trends are dominated by transient dynamics (unpredictability related to initial conditions). The r^* value separating the *very fast* and other regimes therefore constitutes an

r-tipping point.

We note that the *fast* trends case is demographic rate- and trend-specific; in some cases it may be impossible for the delay of a bifurcation to extend towards the end of the trend before entering the realm of *very fast trends*: the r-tipping point then separates *slow* and *very fast* trends.

4 Extensions to other ecological scenarios

Here we demonstrate the generality of our findings with two further examples illustrating common ecological scenarios; the addition of short-term stochastic variation around the long-term environmental trend, and a continuous-time consumer-resource interaction model under a long-term environmental trend that affects mortality rather than reproduction. These examples reinforce our general finding that environmental trends generate r-tipping points and delays in bifurcation leading to b-tipping points, emphasise that our findings are robust to fundamental differences in modelling frameworks, and reveal new insights based on the interaction of short- and long-term environmental change processes. Appendix S1: Section A5 also considers the logistic map under a decreasing environmental trend ($r < 0$).

4.1 Noisy trend

When demographic rates are simultaneously affected by long- and short-term environmental change, the environment is non-stationary and stochastic. We showed that a long-term environmental trend alone delays the reproductive rate (λ_t) at which a density dependent population's abundance starts to cycle: as r increases, so does $b(r)$. Previous work shows how (stationary) fluctuations can "excite" underlying over-compensatory, but stable-point, equilibrium behaviours (e.g., Nisbet and Gurney (1985), Greenman and Benton (2003)). For the logistic map, noise can generate sustained quasi-2-generation cycles at a mean environmental value for $\lambda < 3$ (that we denote $b(n)$), such that $b(n) < 3$, with $b(n)$ decreasing as the variance of the noise n increases (Appendix S1: Section A3). In other words, the short-term noise shifts the bifurcation

$b(n)$ to lower reproductive rates (λ_t), increasingly further into the 'stable' region with higher noise variance. Short-term noise and long-term trends therefore have opposite effects on the onset of observed (quasi-) 2-generation cycles. The joint effects of short- and long-term environmental change on the dynamics of a population undergoing a noisy environmental trend, are related to the concept of "time of emergence" (e.g., Hawkins et al., 2020; Hawkins and Sutton, 2012), which measures the time at which a noisy (often climatic) metric emerges as trendy. The relationship between the time of emergence of a climatic metric and a population's response to it have also been studied previously, in a density-independent framework from which bifurcations and tipping points are absent (Jenouvrier et al., 2022).

Here, we consider a simple extension of equation (3):

$$\begin{cases} n_{t+1} = \lambda_t n_t (1 - n_t) \\ \lambda_t = \bar{\lambda}_t + \epsilon_t \text{ with } \epsilon_t \sim \mathcal{N}(0, \sigma_e^2) \text{ and } \rho(\epsilon) = E\left(\frac{Cov(\epsilon_{t+1}, \epsilon_t)}{\sigma_e^2}\right) \\ \bar{\lambda}_t = \bar{\lambda}_0 + rt \text{ for } 0 \leq t \leq T, \\ \bar{\lambda}_0 = 1.001 \text{ and } \bar{\lambda}_T = 3.9605 \end{cases}, \tag{7}$$

where the value of λ_t, is drawn at each generation, independently and at random from a normal distribution with expected value $\bar{\lambda}_t$, variance σ_e^2 and (one-generation, detrended) expected autocorrelation $\rho(\epsilon)$. For an environmental trend of $r = 0.003$ corresponding to $T = 1000$ generations, we simulated stochastic time-series ϵ_t for various values of σ_e^2 and $\rho(\epsilon)$ (Fig.9). For the deterministic model (Fig.9a), the population starts oscillating at the r-affected b-tipping point $b(r) \approx 3.4$.

For a noisy trend with low stochastic variance ($\sigma_e = 0.01$, Fig.9b), the abundances show pseudo-2-generation cycles earlier than the trend-only case, so that we have a noise and rate induced "bifurcation", that we denote $b(r, \sigma_e)$ such that $3 < b(0.003, 0.01) < b(0.003, 0) \approx 3.4$. This delay in the onset of 2-generation cycles is reduced compared to the deterministic case; yet because of the trend, the onset of underlying oscillations occurs at higher λ_t values than the

constant environment framework bifurcation at $\lambda = 3$. For noise with higher variance ($\sigma_e = 0.05$, Fig.9d), the effect of the noise appears to match or cancel out that of the trend, and the pseudo-2-generation cycles start at $b(0.003, 0.05) \approx 3$. For even larger environmental noise ($\sigma_e = 0.15$, Fig.9f), the short-term noise dominates and $b(0.003, 0.15) < 3$. Positive autocorrelation in the short-term noise has a strong effect on the onset of oscillations, as it reduces the effects of the noise on the dynamics (Figures 9c and 9e).

4.2 A predator-prey model in continuous time

Here we consider a classic predator-prey system (Hsu et al., 1978; Wrzosek, 1990), where the population dynamics are defined by a system of differential equations, with intraspecific density dependence in the prey and a Type II functional response:

$$\begin{cases} \frac{dn_1}{dt} = \lambda n_1(1 - n_1) - n_2 \frac{an_1}{1+ahn_1} \\ \frac{dn_2}{dt} = n_2 \left(c \frac{an_1}{1+ahn_1} - d \right) \end{cases}, \tag{8}$$

where n_1 and n_2 are prey and predator abundances, a is the attack rate (here $a = 0.4$), $c = 0.2$ is the conversion rate, $h = 3$ the handling time, $\lambda = 0.1$ the maximum prey growth rate (in the absence of competition and predation). In this case, we set the density independent predator death rate (d) as the time-varying demographic parameter, decreasing linearly from $d_0 = 0.02$ to $d_T = 0.002$ over a duration of length T, before settling at $d_{t \geq T} = d_T$.

The constant-environment bifurcation diagram shows how the asymptotic predator-prey dynamics vary as a function of predator mortality (d). It is displayed in the background of the superimposition diagrams (middle column, II, Fig. 10), in orange and light blue. For higher death rates $d > d_a \approx 0.01$ (e.g., at d_0), all (positive) trajectories converge towards a two-species stable equilibrium $(\hat{n}_1, \hat{n}_2)$. For lower death rates $d < d_a$, this equilibrium point is unstable and the asymptotic trajectories are limit cycles in constant environments (e.g., at d_T). When predator mortality follows a *very slow* (declining) trend ($T = 750,000$, $r = \frac{d_T - d_0}{T} = -2.410^{-8}$, top row of

Fig.10), prey abundances initially decrease and predator abundances increase slightly, with no or very small oscillations,before starting to oscillate strongly as predator mortality (in orange, right hand y-axis) passes a critical threshold $b(r) < d_a$. The corresponding superimposition diagram (Fig.10aII, to be read from right to left as $r < 0$), shows the system initially tracking the moving equilibrium $(\hat{n}_1(t), \hat{n}_2(t))$ (in black).

As with the single-species discrete time model, there is a delayed bifurcation (d_a): abundances keep tracking the moving equilibrium, which acts as a ghost attractor, for predator death rates corresponding to an unstable point equilibrium in a constant environment, i.e., for $d_t < d_a$. Eventually, a qualitative *and* quantitative regime shift occurs (i.e., a b-tipping point) and the population abundances oscillate with increasing amplitudes. The "catch-up" effect is noticeable: the increase in the magnitude of oscillations is much faster (in the alternative timescale d_t of the superimposition diagram Fig.10aII) than that predicted by the constant environment framework (in orange and cyan). By the end of the environmental trend, the quasi-cycles have the same amplitude as the asymptotic cycle at $d = d_T$, as highlighted on the phase diagram (the continuous time equivalent to the cobweb plots) of Fig. 10aIII where the trend trajectories are in blue (post-trend trajectory in grey and moving equilibrium in yellow): there is no post-trend transient.

The very slow trend contrasts quantitatively with the dynamics under a *slow* trend ($T = 75,000$, second row of Fig.10) where the delay in bifurcation is larger and the quasi-cycles at the end of the trend are much smaller in amplitude that those of the constant environment framework. It takes another $10,000$ time-steps in the post-trend constant environment ($t \geq T$) for the oscillations to reach the asymptotic behaviour (post-trend trajectory in grey). As with the single-species discrete time model, for a *fast* environmental trend ($T = 7,500$; third row of Fig.10), abundances track the moving equilibrium during the entire duration of the trend. Significant oscillations (i.e., of the same order of magnitude as the bifurcation diagram) only occur after the environmental trend has finished ($t \geq T$), and a long transient is required for the abundances to reach the asymptotic cycle, which they do from *inside* that cycle (Fig.10cIII).

This contrasts qualitatively with the dynamics of a *very fast* trend ($T = 20$, lowest row of Fig.10) where the dynamics are driven by the post-trend transient (there is continuity between the trend (blue) and post-trend (grey) trajectories, Fig.10dIII) and the abundances cycle towards the asymptotic orbit from *outside* the attractor. This is a proof of the existence of an $r-$tipping point that segregates rates of environmental change where, on the fast side, abundances track the moving equilibrium and then cycle towards the asymptotic attractor with increasing amplitudes and, on the very fast side, abundances are driven by transient dynamics and cycle, from the start of the trend, with decreasing amplitudes towards the attractor.

5 Mechanisms underlying the delay in bifurcation

In this section, we turn back to the logistic map with trending reproductive rate (eq.3) and provide two approaches to understand mechanistically the observed population dynamics of section 3, and in particular the delay in bifurcations. The first approach is graphical and uses cobweb diagrams (section 5.1). The second approach is mathematical (section 5.2).

5.1 Illustrating the delay in bifurcation with cobweb diagrams

Under an environmental trend, the population dynamics emerge from the combination of *two forces*:

(*i*) the *transient dynamics* pushing abundances n_{t+1} towards the asymptotic behaviour determined by λ_t (i.e., the moving equilibrium $\hat{n}_t$ for $1 < \lambda < 3$), and

(*ii*) the *shift, over time, of that equilibrium* attractor ($\hat{n}_t$ is a "moving" function of t via λ_t, eq.4).

Cobweb diagrams provide a useful way to investigate how these two forces interact to shape population dynamics. Fig.11a illustrates a "classic" constant environment framework, here for a 2-point cycle, corresponding to $\lambda = 3.1$, reached from $n_0 = \hat{n}(\lambda) = 0.6774$. Fig.11b highlights the first 15 generations. The population response (growth) curve $n_{t+1} = f(n_t)$ (in red) and the black

1:1 line yield abundance trajectories (in blue). The response curve crosses the 1:1 curve at the equilibrium: $\hat{n} = 1 - \frac{1}{\lambda}$. This equilibrium is unstable (Fig.1): abundances cycle away towards the asymptotic 2-generation cycle. This trajectory corresponds to that of the *slow* environmental trend (Fig.2) if the trend stopped at $\lambda_t = 3.1$.

Allowing the trend to continue at the *slow* pace (Fig.2), for 10 successive generations around $3 < \lambda_t \approx 3.10 < b(r)$, results in Figure 11c. The temporally changing environment is reflected by multiple (red) population response curves. Abundances (blue) smoothly track the moving equilibrium ($\hat{n}_t$), located where the (red) response curves and the (black) 1:1 line intersect. As the time-varying demographic parameter increases further, the distance between response curves diminishes and abundances start to oscillate (at $\lambda_t \approx b(r)$, Fig.11d). Eventually, they reach values associated with the 2-generation cycle (Figures 11e and 11f). Then, the environment (and response curve) still changes each generation, but this change is so small compared to the amplitude of the cycles, that it can be considered constant over multiple generations. The 15 response curves (the f_t of eq.3a), corresponding to the 15 successive values of λ_t, are almost indistinguishable and, consequently, so are the 15 quasi 2-generation abundance cycles (blue, Fig.11f).

Before the time-varying demographic parameter has reached the b-tipping point (Fig.11c), the abundances track the moving equilibrium closely (with $\hat{n}_{t-1} < n_t < \hat{n}_t$) with a lag:

$$h_t = n_t - \hat{n}_t. \tag{9}$$

This lag (h_t) corresponds to the distance between the realised abundances (in blue) and the moving equilibrium (in red) of the superimposition diagram (Fig.3). On these cobweb diagrams, the lag reflects the distance on the 1:1 line between the abundances (blue) and the response curves (red). Holding λ_t constant (Fig.11b), shows abundances cycling away from the point equilibrium. From $n_{t_1} < \hat{n}_{t_1}$, we would get $\ldots < n_{t_1+2} < n_{t_1} < \hat{n}_{t_1} < n_{t_1+1} < n_{t_1+3} < \ldots$ and the cycle increases in

amplitude until it reaches its asymptotic 2-generation cycle. In contrast, with an environmental trend, the lag is perpetuated because of the distance between the successive response curves, equal to

$$g(r, \lambda_t) = \hat{n}_{t+1} - \hat{n}_t = \frac{r}{\lambda_t(\lambda_t + r)} \approx \frac{r}{\lambda_t^2}, \tag{10}$$

which corresponds to the *speed of the moving equilibrium*. From $\hat{n}_{t_1-1} < n_{t_1} < \hat{n}_{t_1}$, we therefore get $\hat{n}_{t_1} < n_{t_1+1}$. Then, as $g(r, \lambda_t) > n_{t_1+1} - \hat{n}_t$, we have $n_{t_1+1} < \hat{n}_{t_1+1}$, and so on: as long as the speed of the moving equilibrium, $g(r, \lambda_t)$, is large enough, the population abundance tracks the moving equilibrium with a lag. For a given rate of environmental change r, the distance between successive abundance attractors, $g(r, \lambda_t)$, diminishes over time, as λ_t increases (eq.10), so that at the onset of oscillations (t_o, as λ_t passes the b-tipping point $b(r)$), the lag is no longer perpetuated and the abundances start cycling (Figures 11d and 11e; see Appendix S1: Section A2).

5.2 Mathematical analysis along the reproductive rate line

The key to better understand the behaviour of abundances under an environmental trend is to consider the distance of the abundances n_t to the "moving equilibrium" $\hat{n}_t$ (eq.(4)), that is, $h_t = n_t - \hat{n}_t$ (eq.(9)), and to analyse its dynamics as a function of the Jacobian and the speed of change of the "moving equilibrium". In the vicinity of $\hat{n}_t$, we can write, via first degree Taylor approximation,

$$n_{t+1} - \hat{n}_t \approx J(\hat{n}_t)(n_t - \hat{n}_t), \tag{11}$$

where $J(\hat{n}_t)$ is the Jacobian of the projection function f, $n_{t+1} = f(n_t)$ (eq.1), evaluated at $\hat{n}_t$. This implies, as $h_{t+1} = n_{t+1} - \hat{n}_t + (\hat{n}_t - \hat{n}_{t+1})$, that for small h_t,

$$h_{t+1} \approx J(\hat{n}_t)h_t + (\hat{n}_t - \hat{n}_{t+1}). \tag{12}$$

In a uni-variate framework, such as the one we are considering here, the Jacobian is simply the derivative and for the logistic map, $f(x) = \lambda_t x(1-x)$, so that $J(x) = \lambda_t(1-2x)$ and

$$J(\hat{n}_t) = 2 - \lambda_t, \tag{13}$$

from eq.(4). Therefore for the logistic map under a trend (eq.3a), equation 12 becomes

$$h_{t+1} \approx (2-\lambda_t)h_t + \frac{\lambda_t - \lambda_{t+1}}{\lambda_{t+1}\lambda_t}, \tag{14}$$

In Appendix S1: Section A4, we use equation (14) to exhibit non-linear trends where abundances remain at a constant distance from the "moving equilibrium". For a linear trend (eq.3b), equation (14) becomes

$$h_{t+1} \approx (2-\lambda_t)h_t - \frac{r}{\lambda_{t+1}\lambda_t} \approx (2-\lambda_t)h_t - \frac{r}{\lambda_t^2}, \tag{15}$$

In all three of these equations (eqs (12),(14) and (15)), the first term corresponds to the Jacobian and the second term to the speed of change of the "moving equilibrium". Here we study the behaviour of n_t, via that of h_t (eq.(15)) for various sections of the λ_t parameter line.

For $1 \leq \lambda_t \leq 2$, h_t goes from 0 to the vicinity of 0 via a dip

The populations are initiated at $\lambda_0 = 1.001$ and $n_0 = \hat{n}_0$, therefore we have $h_0 = 0$. At the next generation, we have, according to equation (15), $h_1 \approx -r$. At the following generation, $h_2 \approx -2r$, etc. The distance h_t, negative, decreases (in absolute value) initially, and all the more so that the trend is fast (that r is high). It is complex to follow up the dynamics after that initial dip (h_t is not small enough for eq.(14) to be valid). However, as one reaches t_2, such that $\lambda(t_2) = 2$, from eq.(15), we get that:

$$h_{t_2+1} \approx (2-\lambda_{t_2})h_{t_2} - \frac{r}{\lambda_{t_2}^2} \approx -\frac{r}{4} \tag{16}$$

At $\lambda_t = 2$, the distance h_t between the “moving equilibrium” and the actual abundance is independent from the trajectory so far (and therefore from the choice of λ_0). It is negative and

small (four times smaller than h_1); the slower the trend, the smaller that distance; i.e., any initial difference between the projected population size n_t and the moving equilibrium $\hat{n}_t$ quickly shrinks.

For $2 \leq \lambda_t \leq 3$, repelling boundaries with an overcompensatory attractor

Going one time-step further, we get $h_{t_2+2} \approx -\frac{r}{4}(1-r)$. The lag h_t remains negative but now decreases (in absolute value) monotonically. We can show, that for h_t for $2 < \lambda_t < 3$ (see below), h_t is constrained by two repelling boundaries:

$$\underbrace{-\frac{r}{\lambda_t^2}}_{l_2(t)} \leq h_t \leq \underbrace{0}_{l_1}. \tag{17}$$

which constrains h_t inside a range of ever decreasing amplitude, so that in this range, for most values of r, we have a *ghost equilibrium* $n_t \approx \hat{n}_t$. In fact, we have, from eq.(17), $\hat{n}_{t-1} \leq n_t \leq \hat{n}_t$, in which we recognise, the initial step of our cobweb diagram analysis. Figure 12, displays h_t for a *slow* trend ($r \approx 1.5 \times 10^{-4}$) in blue, and the boundaries. We also display, in red, $h_2(t)$ for a trajectory that has been artificially disturbed: $h_2(t_p) = 0$ ($\lambda_{t_p} = 2.92$). After the perturbation, $h_2(t)$ is repelled by both boundaries.

Nested functions

We have denoted $\hat{n}_t$, the value of n_t where $n_{t+1} = n_t$. Similarly, let us denote $\hat{h}_t$, the value of h_t so that $h_{t+1} = h_t$. From eq.(15), we can approximate it as

$$\hat{h}_t \approx \frac{-r}{\lambda_t^2(\lambda_t - 1)}, \tag{18}$$

and, as per eq. (9), we can now consider the distance

$$g_t = h_t - \hat{h}_t \tag{19}$$

With the same reasoning on g_t as that on h_t, it can be shown that g_t follows a narrow range in

$2 < \lambda_t < 3$ with one boundary being $\hat{h}_t$, so that if at a first approximation $n_t \approx \hat{n}_t$, at a second approximation

$$h_t \approx \hat{h}_t, \tag{20}$$

that is $n_t \approx \hat{n}_t - \hat{h}_t$. At a third approximation, we could be more precise and write $n_t \approx \hat{n}_t - \hat{h}_t - \hat{g}_t$, with $\hat{g}_t$ the value of g_t so that $g_{t+1} = g_t$, then consider $i_t = g_t - \hat{g}_t$, etc. At t_3 (such that $\lambda_{t_3} = 3$), eq.(20) leads to

$$h_{t_3} \approx \frac{-r}{\lambda_t^2(\lambda_t - 1)} = \frac{-r}{18}$$

For $3 \leq \lambda_t < 4$, cascading effects

For $\lambda_t > 3$, the induction leading to the boundaries of eq.(17) does not hold any longer (see below). At a time t_h, which is an increasing function of r, h_t starts oscillating around $\hat{h}$. This leads, quickly, to a time $t_o > t_h$ where h_t is expelled outside the boundaries (see Figure 12), and therefore $h_{t_o} \geq 0$, that is $n_{t_o} > \hat{n}_{t_o}$ which, from eq.(11) leads to $n_{t_o+1} - \hat{n}_{t_0} < 0$: at t_o, n_t has started oscillating. Considering, the nested functions further, one has $... < t_i < t_b < t_h < t_o$, where t_i (respectively t_g) corresponds to the generation at which i_t (respectively g_t) starts oscillating. As i_t is expelled from its boundaries at t_g, g_t starts oscillating before itself being expelled from its boundaries at t_h, and so on. This corresponds to a cascading effect, that we illustrate in Figure 13, which displays, for the same trend as Fig.12, and for a portion of the trajectory, g_t, h_t and n_t (on log scale to correct for their mean).

Induction on Repelling Boundaries

We have (eq.16), $h_{t_2} \approx h_{t_2+1} \approx -\frac{r}{\lambda_{t_2}^2}$, so that $l_2(t_2) \leq h_{t_2} \leq l_1$. Consider now that for a given t, we have $l_2(t) \leq h_t \leq l_1$. From the right side of that inequality, $h_t \leq l_1$, and from eq.15, we get the left side of the same equation at the next generation:

$$h_{t+1} \approx (2 - \lambda_t)h_t - \frac{r}{\lambda_t\lambda_{t+1}} \geq (2 - \lambda_t)l_1 - \frac{r}{\lambda_t\lambda_{t+1}} = -\frac{r}{\lambda_t\lambda_{t+1}} = l_2(t+1)$$

From the left side of that inequality, $l_2(t) \leq h_t$, and from eq.(15), we get the right side of the same equation at the next generation: for $2 \leq \lambda_t \leq 3$,

$$h_{t+1} \approx (2-\lambda_t)h_t - \frac{r}{\lambda_t^2} \leq (2-\lambda_t)l_2(t) - \frac{r}{\lambda_t^2} \approx -(2-\lambda_t)\frac{r}{\lambda_t^2} - \frac{r}{\lambda_t^2} = -\frac{r}{\lambda_t^2}(3-\lambda_t) \leq 0$$

For all t, $2 < \lambda_t < 3$ and (for a speed of environmental change r that is not too fast, see below), we have

$$l_2(t) \leq h_t \leq l_1, \tag{17}$$

which constrains h_t inside a range of ever decreasing amplitude $l_1 - l_2(t) = \frac{r}{\lambda_t^2}$, so that indeed, at first sight, in this range, for most values of r, we have $n_t \approx \hat{n}_t$. Indeed, inequality 17 can also be written:

$$\hat{n}_{t-1} \leq n_t \leq \hat{n}_t, \tag{21}$$

in which we recognise the inequality resulting from the inspection of the cobweb diagram. From this, we can conclude that l_1 and $l_2(t)$ are repelling boundaries of the abundance trajectory for $2 < \lambda_t < 3$, as per Fig.12.The induction above is loose. Focusing on $l_1 = 0$ and $l_2(t) = -\frac{r}{\lambda_t \lambda_{t-1}}$, we get, from $l_2(t) \leq h_t \leq l_1$ at the next generation $h_{t+1} \geq -\frac{r}{\lambda_t \lambda_{t+1}} = l_2(t+1)$ from from eq.15. From the same equation, we also have $h_{t+1} \leq (\lambda_t - 2)\frac{r}{\lambda_t \lambda_{t-1}} - \frac{r}{\lambda_t \lambda_{t+1}}$. This expression is negative for most of the $2 \leq \lambda_t \leq 3$ range. It becomes positive when $(\lambda_t - 2)\frac{r}{\lambda_t \lambda_{t-1}} = \frac{r}{\lambda_t \lambda_{t+1}}$ that is, when $(\lambda_t - 2)(\lambda_t + r) = \lambda_t - r$, which corresponds to $\lambda_t = \frac{3-r}{2} + \sqrt{r + \left(\frac{3-r}{2}\right)^2}$ which is very close to 3 for most values of r.

6 Discussion

We have explored the dynamical consequences of the rate of change of an environmentally driven demographic parameter for density-dependent populations, in discrete- and continuous-time, under coupled short- and long-term environmental change and with a trophic interaction. We characterised four rates of long-term environmental change, corresponding to qualitatively and

quantitatively different combinations of dynamical behaviours across these different, but familiar ecological scenarios, and related our findings to recent developments in the study of regime shifts in ecological dynamics – long transients and tipping points.

Long transients

The dynamics of *very fast* trends were mainly influenced by transient dynamics. This qualitative regime appears for the highest rates of environmental change, where $r > r^*$ (the *r-tipping point*), in the *r-bifurcation diagram* (fig. 7). Here, the population did not track the environment, but showed highly unpredictable transient duration and amplitude range (fig. 7 and fig.S3 of SMA1). The ecological behaviour of such (potentially) "long transients" has recently been described for various types of attractors, including showing how the transient can push the population below pseudo-extinction thresholds from abundant population sizes and/or on the way to an attractor corresponding to high abundances, affecting population resilience (e.g., Baker and Röst, 2020; Poggiale, 2020; Rubin et al., 2022; Morozov et al., 2016; Rubin et al., 2022; Morozov et al., 2020, 2024).

Most of the reproductive parameter values of the logistic map ($1 < \lambda \lesssim 3.57$) lead to unique attractors (stable point or n-point cycling equilibrium points) which are approached by any initial population abundance ($0 < n_0 < 1$); as such the abundance trajectories are not subject to the chaotic supertransients typical of spatio-temporal dynamical systems (Lai and Tél, 2011). We showed that certain rates of environmental change led to unpredictable abundance dynamics and transient durations, both during and after the environmental trend. However, one of our main findings is that this behaviour is limited to a specific range that corresponds to *very fast* environmental trends with respect to the natural speed of the system (fig.7), (i.e., the natural fluctuations of demographic rates, here the fertility rate λ_t, which is not expected to transition from its minimal value ($\lambda_t \gtrsim 1$) to its maximum value ($\lambda_t \lesssim 4$) in a matter of a few generations, Vanselow et al., 2019). For *very fast* trends, the dynamics are driven by the transient, which is sensitive to initial conditions and therefore very hard to predict.

r-tipping points, delays in bifurcation and b-tipping points

When the environmental rate of change was slower than r^*, population abundances initially appeared to behave according to the constant environment framework; i.e., following the bifurcation diagram which, for the logistic map, predicts a monotonic increase in long-term abundances ($\hat{n}, \lambda < 3$) followed by oscillations ($\lambda > 3$). In other words, the rate of environmental change was slow enough for the abundances to track the environment. This situates r^* as a bifurcation on an r-bifurcation diagram, or *r-tipping point*, segregating two qualitatively different regimes (Ashwin et al., 2012; Siteur et al., 2016; Ritchie et al., 2023; Vanselow et al., 2022; Abbott et al., 2024). We showed, however, that the effect of r on the dynamics goes beyond the r-tipping point. On the slower side of r^*, abundances track the environment, in the shape of the moving equilibria corresponding to the attractors of the bifurcation diagram (Hastings et al., 2018). However, because of the environmental trend, the bifurcations are delayed: in the case of the logistic map with increasing reproductive rate (λ_t), the population abundances start oscillating at a higher λ_t than the bifurcation point in the constant environment.

If the reproductive rate decreases over time (i.e., $r < 0$), the bifurcation is again delayed, but in the opposite direction: the population *stops* oscillating at lower reproductive rates ($\lambda_t < 3$; SMA5). During these *bifurcation delays*, the moving equilibrium tracked by the abundances does not correspond, in the constant environment framework, to a stable equilibrium; it is a *ghost equilibrium*. In ecology, delayed bifurctions have rarely been investigated, with the exception of extinction (transcritical) bifurcations (Zarada and Drake, 2017; Drake and Griffen, 2010). However, delayed bifurcations have been studied extensively in other non-ecological contexts (e.g., Wu and Wang, 2017; Su, 2001; Wei et al., 2008; Baer et al., 1989; Miyazaki and Tchizawa, 2005).

The bifurcation delay is accompanied by a catch-up effect: abundances quickly jump from the ghost equilibrium to the next equilibrium (corresponding to the 2-generation cycles, when considering the $\lambda = 3$ bifurcation at of the logistic map with increasing reproductive rate). This leads to an abrupt qualitative and quantitative change of regime for the abundances: a *b-tipping*

point; *b*-tipping points are generally associated with complex (discontinuous) bifurcations where, e.g., on one side of the bifurcation, there is no equilibrium (Boettiger and Batt, 2020; Scheffer et al., 2001; Dakos et al., 2012; Boettiger and Hastings, 2012).

We showed that *b*-tipping points can also occur for the simpler (continuous), period-doubling bifurcations of the logistic map, where passing the bifurcation leads to an abrupt regime change. This implies that while the trend is slow enough for the abundances to track the environment, they can track different versions of the environment for the same value of the environmentally driven parameter, as a function of the environmental rate of change. That is, they track different moving equilibria/ghost attractors, and rapidly shift between them to generate *b*-tipping points.

For the logistic map with increasing reproductive rate over time ($r > 0$), the abundances track the unstable (ghost) point equilibrium up to the first *b*-tipping point and the stable 2-generation cycle thereafter, with the change of regime occurring very rapidly. In summary, we defined *very fast* trends, for a given demographic rate and related bifurcation, as environmental trends leading to population dynamics dominated by transients. On the slower side of the *r-tipping point*, *fast* trends correspond to cases where no bifurcation occurs (despite the temporally-changing demographic rate passing the value of the constant-environment bifurcation). In *slow* trends, the bifurcation is also delayed, but this delay occurs before the end of the trend. *Very slow* trends are a special case of *slow* trends where the rate of environmental change is slow enough to avoid any post-trend transient.

Risks of simplifying frameworks

Overall, we showed that a population's trajectory under an environmental trend is the result of two forces: the transient approach towards the asymptotic environmental attractor and the constant temporal shift of that attractor (it is "moving"). The population trajectory cannot, therefore, be understood by considering only the asymptotic abundances based on the bifurcation diagram, nor the transient dynamics approaching these asymptotic abundances. Focusing solely on the

asymptotic behaviour in two distinct, constant environments, as ecologists sometimes do to anticipate population responses to global change, reduces the validity of such studies to unrealistically slow trends. Focusing solely on the latter (transients), by considering an instantaneous change between the initial and the long-term value of the environment following the transient dynamics framework, is equally risky as it limits the validity range to unrealistically fast trends.

We have shown here, that considering both, in the hope that a realistic trend will behave in an intermediate way between a *very fast* and a *very slow* trend, is not satisfactory either: it prevents us from observing the existence of an r-tipping point and the emergence of simple bifurcations as b-tipping points. However, while simplifying assumptions are an unavoidable part of ecological modelling, the most important risk lies in not expressing them explicitly when interpreting results (Scheiner, 2013).

A general perspective and a toolkit for ecologists

We considered simple population models with linear trends in demographic rates, but note that the approach can easily be extended to non-linear trends (SMA4). Our approach does not correspond to a specific system or environmental trend but provides a general framework under which to study any population model under environmental change; including those implemented experimentally (generally, over relatively short timescales, e.g., Tabi et al., 2020). A researcher equipped with a population projection model and the functional responses of relevant demographic rates to environmental cues will be able, via the *r-bifurcation diagram*, to get a broader picture of the future population dynamics under different environmental trend scenarios, and identify r-tipping points. For a given scenario, the *superimposition diagram* will highlight the consequences of passing certain (even simple, continuous) bifurcations and the potential regime shifts, or b-tipping points, it may lead to. We hope these tools and this framework will allow more complete investigations into population or community resilience to the ongoing global changes of uncertain speeds.

For example, global change has important impacts on sea temperature and ocean acidification, in turn, affecting critical ecosystem services provided by fisheries (Jørgensen et al., 2020; Mondal and Lee, 2025). These long-term trends, for which the IPCC has proposed several scenarios in terms of magnitude and duration (Diop et al., 2018; Cheung et al., 2016), impact the recruitment of fish populations (Shoji et al., 2011; Mondal and Lee, 2025) and therefore the stocks which leads to various trends in fishing pressure (Hilborn et al., 2022).

Projection models have been developed for various populations, communities or areas, embedding the response of recruitment to these gradual changes in temperature, acidity and/or fishing pressure (Sadykov et al., 2022; Brooks, 2024; Maunder and Thorson, 2019). They can further incorporate life-history evolution (McKeon et al., 2024) and spatial structure (incorporating the "tropicalization" of fishing areas, e.g., Cheung et al., 2013). From these inputs, the consequences of the rate of environmental change on fish populations can be studied via *superimposition diagrams*; they can provide crucial information on potential b-tipping points, delays in bifurcation, and more generally the possibility of abrupt regime shifts in the abundance and distribution of fish stocks. The *r-bifurcation diagram*, considering the speeds of these various trends on a continuum (considered individually or jointly), yields important information on the effects of various global change and fishing policy scenarios on long-term fish stock dynamics. It would inform on both the dynamics during and after the trend, allowing predictions of what abundance levels and how fast, fish stocks are expected to stabilise once/if CO_2 emissions are significantly reduced.

While we have focussed on the dynamics of density dependent population abundances under (linear) environmental trends, we believe the approach and associated analytical tools, will generalise to models of trait or other dynamics and a wide range of environmental change scenarios. This should allow novel hypotheses to be developed and compared around constant *vs.* changing environments, helping us to determine the importance of the existence and rates of temporal environmental change on ecological and evolutionary dynamics.

Acknowledgements:

This research was funded by the Natural Environment Research Council (grant no. NE/W006731/1) awarded to MSF, SMS, and CY.

Statement of authorship: CFDC, BP, SMS and MSF initiated the project. CFDC, BP and MSF performed simulations. CFDC and CY developed the mathematical analyses. CFDC and MSF led the writing of the manuscript. All authors contributed to the final version of the manuscript.

Conflict of interest: The authors declare no conflict of interests.

References

Abbott, K. C., Heggerud, C. M., Lai, Y. C., Morozov, A., Petrovskii, S., Cuddington, K., and Hastings, A. (2024). When and why ecological systems respond to the rate rather than the magnitude of environmental changes. *Biological Conservation*, 292.

Agrell, J., Erlinge, S., Nelson, J., Nilsson, C., and Persson, I. (1995). Delayed density-dependence in a small-rodent population. *Proceedings of the Royal Society B: Biological Sciences*, 262(1363):65–70.

Ashwin, P., Wieczorek, S., Vitolo, R., and Cox, P. (2012). Tipping points in open systems: Bifurcation, noise-induced and rate-dependent examples in the climate system. *Philosophical Transactions of the Royal Society A: Mathematical, Physical and Engineering Sciences*, 370(1962):1166–1184.

Baer, S. M., Erneux, T., and Rinzel, J. (1989). The Slow Passage through a Hopf Bifurcation: Delay, Memory Effects, and Resonance. *SIAM Journal on Applied Mathematics*, 49(1):55–71.

Baker, R. E. and Röst, G. (2020). Global Dynamics of a Novel Delayed Logistic Equation Arising from Cell Biology. *Journal of Nonlinear Science*, 30(1):397–418.

Barraquand, F., Louca, S., Abbott, K. C., Cobbold, C. A., Cordoleani, F., DeAngelis, D. L., Elderd, B. D., Fox, J. W., Greenwood, P., Hilker, F. M., Murray, D. L., Stieha, C. R., Taylor, R. A., Vitense, K., Wolkowicz, G. S., and Tyson, R. C. (2017). Moving forward in circles: challenges and opportunities in modelling population cycles. *Ecology Letters*, 20(8):1074–1092.

Boettiger, C. and Batt, R. (2020). Bifurcation or state tipping: assessing transition type in a model trophic cascade. *Journal of Mathematical Biology*, 80(1-2):143–155.

Boettiger, C. and Hastings, A. (2012). Quantifying limits to detection of early warning for critical transitions. *Journal of the Royal Society Interface*, 9(75):2527–2539.

Brauer and Castillo-Chavez (2013). *Mathematical Models in Population Biology and Epidemiology*, volume 53.

Brooks, E. N. (2024). Pragmatic approaches to modeling recruitment in fisheries stock assessment: A perspective. *Fisheries Research*, 270(November 2023):106896.

Burc, E., Girard-Tercieux, C., Metz, M., Cazaux, E., Baur, J., Koppik, M., Rêgo, A., Hart, A., and Berger, D. (2025). Life-history adaptation under climate warming magnifies the agricultural footprint of a cosmopolitan insect pest. *Nature Communications*.

Burke, K. D., Williams, J. W., Chandler, M. A., Haywood, A. M., Lunt, D. J., and Otto-Bliesner, B. L. (2018). Pliocene and Eocene provide best analogs for near-future climates. *Proceedings of the National Academy of Sciences of the United States of America*, 115(52):13288–13293.

Campbell, R. D., Nouvellet, P., Newman, C., MacDonald, D. W., and Rosell, F. (2012). The influence of mean climate trends and climate variance on beaver survival and recruitment dynamics. *Global Change Biology*, 18(9):2730–2742.

Carpenter, S. R., Cole, J. J., Pace, M. L., Batt, R., Brock, W. A., Cline, T., Coloso, J., Hodgson,

J. R., Kitchell, J. F., Seekell, D. A., Smith, L., and Weidel, B. (2011). Early Warnings of Regime Shifts: A Whole-Ecosystem Experiment. *Science*, 332(6033):1079–1082.

Caswell, H. and Werner, P. A. (1978). Transient Behavior and Life History Analysis of Teasel (Dipsacus Sylvestris Huds.). *Ecology*, 59(591):53–66.

Cheung, W. W., Watson, R., and Pauly, D. (2013). Signature of ocean warming in global fisheries catch. *Nature*, 497(7449):365–368.

Cheung, W. W. L., Reygondeau, G., and Frölicher, T. L. (2016). Large benefits to marine fisheries of meeting the 1.5°C global warming target. *Science*, 354(6319):1591–1594.

Chevin, L.-M., Cotto, O., and Ashander, J. (2017). Stochastic Evolutionary Demography under a Fluctuating Optimum Phenotype. *The American Naturalist*, pages 000–000.

Cohen, J. M., Lajeunesse, M. J., and Rohr, J. R. (2018). A global synthesis of animal phenological responses to climate change. *Nature Climate Change*, 8(3): 224–228.

Dakos, V., Carpenter, S. R., Brock, W. A., Ellison, A. M., Guttal, V., Ives, A. R., Kéfi, S., Livina, V., Seekell, D. A., van Nes, E. H., and Scheffer, M. (2012). Methods for detecting early warnings of critical transitions in time series illustrated using simulated ecological data. *PLoS ONE*, 7(7).

Diop, B., Sanz, N., Duplan, Y. J. J., Guene, E. H. M., Blanchard, F., Pereau, J. C., and Doyen, L. (2018). Maximum Economic Yield Fishery Management in the Face of Global Warming. *Ecological Economics*, 154(June 2018):52–61.

Drake, J. M. and Griffen, B. D. (2010). Early warning signals of extinction in deteriorating environments. *Nature*, 467(7314):456–459.

Elton, C. and Nicholson, M. (1942). The Ten-Year Cycle in Numbers of the Lynx in Canada. *The Journal of Animal Ecology*, 11(2):215.

Francis, T. B., Abbott, K. C., Cuddington, K., Gellner, G., Hastings, A., Lai, Y. C., Morozov, A., Petrovskii, S., and Zeeman, M. L. (2021). Management implications of long transients in ecological systems. *Nature Ecology and Evolution*, 5(3):285–294.

Gil, M. A., Baskett, M. L., Munch, S. B., and Hein, A. M. (2020). Fast behavioral feedbacks make ecosystems sensitive to pace and not just magnitude of anthropogenic environmental change. *Proceedings of the National Academy of Sciences of the United States of America*, 117(41):25580–25589.

Gilljam, D., Knape, J., Lindén, A., Mugabo, M., Sait, S. M., and Fowler, M. S. (2019). The colour of environmental fluctuations associated with terrestrial animal population dynamics. *Global Ecology and Biogeography*, 28(2):118–130.

Graham, I. M. and Lambin, X. (2002). The impact of weasel predation on cyclic field-vole survival: The specialist predator hypothesis contradicted. *Journal of Animal Ecology*, 71(6):946–956.

Greenman, J. V. and Benton, T. G. (2003). The amplification of environmental noise in population models: Causes and consequences. *American Naturalist*, 161(2):225–239.

Hansen, J., Sato, M., Ruedy, R., Lo, K., Lea, D. W., and Medina-Elizade, M. (2006). Global temperature change. *Proceedings of the National Academy of Sciences of the United States of America*, 103(39):14288–14293.

Hastings, A., Abbott, K. C., Cuddington, K., Francis, T., Gellner, G., Lai, Y. C., Morozov, A., Petrovskii, S., Scranton, K., and Zeeman, M. L. (2018). Transient phenomena in ecology. *Science*, 361(6406).

Hawkins, E., Frame, D., Harrington, L., Joshi, M., King, A., Rojas, M., and Sutton, R. (2020). Observed Emergence of the Climate Change Signal: From the Familiar to the Unknown. *Geophysical Research Letters*, 47(6).

907 Hawkins, E. and Sutton, R. (2012). Time of emergence of climate signals. *Geophysical Research*
908 *Letters*, 39(1):1–6.

909 Highland, S. A. and Jones, J. A. (2014). Extinction debt in naturally contracting mountain
910 meadows in the Pacific Northwest, USA: Varying responses of plants and feeding guilds of
911 nocturnal moths. *Biodiversity and Conservation*, 23(10):2529–2544.

912 Hilborn, R., Buratti, C. C., Díaz Acuña, E., Hively, D., Kolding, J., Kurota, H., Baker, N., Mace,
913 P. M., de Moor, C. L., Muko, S., Osio, G. C., Parma, A. M., Quiroz, J. C., and Melnychuk,
914 M. C. (2022). Recent trends in abundance and fishing pressure of agency-assessed small
915 pelagic fish stocks. *Fish and Fisheries*, 23(6):1313–1331.

916 Hsu, S. B., Hubbell, S. P., and Waltman, P. (1978). Competing Predators. *SIAM Journal on*
917 *Applied Mathematics*, 35(4):617–625.

918 Ives, A. R. and Carpenter, S. R. (2007). Stability and diversity of ecosystems. *Science*,
919 317(5834):58–62.

920 Jenouvrier, S., Long, M. C., Coste, C. F. D., Holland, M., Gamelon, M., Yoccoz, N. G., and
921 Sæther, B.-e. E. (2022). Detecting climate signals in populations across life histories. *Global*
922 *Change Biology*, 28(7):2236–2258.

923 Johnson, C. A., Ren, R., and Buckley, L. B. (2023). Temperature Sensitivity of Fitness
924 Components across Life Cycles Drives Insect Responses to Climate Change. *The American*
925 *Naturalist*, 202(6):753–766.

926 Jørgensen, L. L., Bakke, G., and Hoel, A. H. (2020). Responding to global warming: New
927 fisheries management measures in the Arctic. *Progress in Oceanography*, 188(August):102423.

928 Kemp, D. B., Eichenseer, K., and Kiessling, W. (2015). Maximum rates of climate change are
929 systematically underestimated in the geological record. *Nature Communications*, 6.

930 Kiritani, K. (2013). Different effects of climate change on the population dynamics of insects.

Korpimäki, E., Oksanen, L., Oksanen, T., Klemola, T., Norrdahl, K., and Banks, P. B. (2005). Vole cycles and predation in temperate and boreal zones of Europe. *Journal of Animal Ecology*, 74(6):1150–1159.

Krebs, C. J. (1995). Two paradigms of population regulation. *Wildlife Research*, 22(1):1–10.

Lai, Y.-C. and Tél, T. (2011). *Transient Chaos: Complex Dynamics on Finite Time Scales (Applied Mathematical Sciences)*.

Lawson, C. R., Vindenes, Y., Bailey, L., and van de Pol, M. (2015). Environmental variation and population responses to global change. *Ecology Letters*, 18(7):724–736.

Le Treut, H. and Somerville, R. (2007). Historical Overview of Climate Change Science Coordinating Lead Authors: Lead Authors. In *Climate Change 2007: The Physical Science Basis. Contribution of Working Group I to the Fourth Assessment Report of the Intergovernmental Panel on Climate Change*.

Lear, C. H., Anand, P., Blenkinsop, T., Foster, G. L., Gagen, M., Hoogakker, B., Larter, R. D., Lunt, D. J., McCave, I. N., McClymont, E., Pancost, R. D., Rickaby, R. E., Schultz, D. M., Summerhayes, C., Williams, C. J., and Zalasiewicz, J. (2020). Geological society of london scientific statement: What the geological record tells us about our present and future climate. *Journal of the Geological Society*, 178(1).

Lee, A. M., Sæther, B. E., and Engen, S. (2020). Spatial covariation of competing species in a fluctuating environment. *Ecology*, 101(1):1–9.

Levin, S. A. (1976). Population Dynamic Models in Heterogeneous Environments. *Annual Review of Ecology and Systematics*, 7(1):287–310.

Maunder, M. N. and Thorson, J. T. (2019). Modeling temporal variation in recruitment in fisheries stock assessment: A review of theory and practice. *Fisheries Research*, 217(June 2018):71–86.

May, R. M. (1974). Biological Populations with Nonoverlapping Generations: Stable Points, Stable Cycles, and Chaos. *Science*, 186(4164):645–647.

May, R. M. (1976). Simple mathematical models with very complicated dynamics. *Nature*, 261(5560):459–467.

McKeon, C. M., Buckley, Y. M., Moriarty, M., Lundy, M., and Kelly, R. (2024). Increased signal of fishing pressure on community life-history traits at larger spatial scales. *Global Ecology and Biogeography*, 33(5):1–17.

Mitani, N. and Mougi, A. (2017). Population cycles emerging through multiple interaction types. *Royal Society Open Science*, 4(9).

Miyazaki, R. and Tchizawa, K. (2005). Bifurcation delay in a delay differential equation. *Nonlinear Analysis, Theory, Methods and Applications*, 63(5-7):3–5.

Mondal, S. and Lee, M.-A. (2025). Impact of Global Warming on Fisheries. In *Food Security, Nutrition and Sustainability Through Aquaculture Technologies*, pages 227–253. Springer Nature Switzerland, Cham.

Morozov, A., Abbott, K., Cuddington, K., Francis, T., Gellner, G., Hastings, A., Lai, Y. C., Petrovskii, S., Scranton, K., and Zeeman, M. L. (2020). Long living transients: Enfant terrible of ecological theory?: Reply to comments on "Long transients in ecology: Theory and applications". *Physics of Life Reviews*, 32:55–58.

Morozov, A. Y., Almutairi, D., Petrovskii, S. V., and Hastings, A. (2024). Regime shifts, extinctions and long transients in models of population dynamics with density-dependent dispersal. *Biological Conservation*, 290(November 2023):110419.

Morozov, A. Y., Banerjee, M., and Petrovskii, S. V. (2016). Long-term transients and complex dynamics of a stage-structured population with time delay and the Allee effect. *Journal of Theoretical Biology*, 396:116–124.

Myers, J. H. (2018). Population cycles: Generalities, exceptions and remaining mysteries. *Proceedings of the Royal Society B: Biological Sciences*, 285(1875).

Nisbet, R. M. and Gurney, W. S. C. (1985). *Modelling fluctuating populations*, volume 4.

Olonscheck, D., Schurer, A. P., Lücke, L., and Hegerl, G. C. (2021). Large-scale emergence of regional changes in year-to-year temperature variability by the end of the 21st century. *Nature Communications*, 12(1):2–11.

Ovaskainen, O. and Hanski, I. (2002). Transient Dynamics in Metapopulation Response to Perturbation. *Theoretical Population Biology*, 61(3):285–295.

Poggiale, J. C. (2020). Regime shifts at the origin of a long transient methodological development for predictive ecology: Comment on "Long transients in ecology: Theory and applications" by A. Morozov et al. *Physics of Life Reviews*, 32:50–52.

Ratikainen, I. I., Gill, J. A., Gunnarsson, T. G., Sutherland, W. J., and Kokko, H. (2008). When density dependence is not instantaneous: Theoretical developments and management implications. *Ecology Letters*, 11(2):184–198.

Ritchie, P. D., Alkhayuon, H., Cox, P. M., and Wieczorek, S. (2023). Rate-induced tipping in natural and human systems. *Earth System Dynamics*, 14(3):669–683.

Rogers, T. L., Johnson, B. J., and Munch, S. B. (2022). Chaos is not rare in natural ecosystems. *Nature Ecology and Evolution*, 6(8):1105–1111.

Roughgarden, J. (1975). A Simple Model for Population Dynamics in Stochastic Environments. *The American Naturalist*, 109(970):713–736.

Royama, T. (1992). *Analytical Population Dynamics*.

Rubin, J. E., Earn, D. J., Greenwood, P. E., Parsons, T. L., and Abbott, K. C. (2022). Irregular population cycles driven by environmental stochasticity and saddle crawlbys. *Oikos*, pages 1–17.

Ruokolainen, L., Lindén, A., Kaitala, V., and Fowler, M. S. (2009). Ecological and evolutionary dynamics under coloured environmental variation. *Trends in Ecology and Evolution*, 24(10):555–563.

Sadykov, A., Farnsworth, K., Sadykova, D., and Stenseth, N. C. (2022). The transfer function method reveals how age-structured populations respond to environmental fluctuations with serious implications for fisheries management. *Population Ecology*, (May 2021):1–15.

Saether, B.-E., Coulson, T., Grøtan, V., Engen, S., Altwegg, R., Armitage, K. B., Barbraud, C., Becker, P. H., Blumstein, D. T., Dobson, F. S., Festa-Bianchet, M., Gaillard, J.-M., Jenkins, A., Jones, C., Nicoll, M. A. C., Norris, K., Oli, M. K., Ozgul, A., and Weimerskirch, H. (2013). How Life History Influences Population Dynamics in Fluctuating Environments. *The American Naturalist*, 182(6):743–759.

Sæther, B. E., Tufto, J., Engen, S., Jerstad, K., Røstad, O. W., and Skatan, J. E. (2000). Population dynamical consequences of climate change for a small temperate songbird. *Science*, 287(5454):854–856.

Sage, R. F. (2020). Global change biology: A primer. *Global Change Biology*, 26(1):3–30.

Scheffer, M., Straile, D., van Nes, E. H., and Hosper, H. (2001). Climatic warming causes regime shifts in lake food webs. *Limnology and Oceanography*, 46(7):1780–1783.

Scheffer, M., Carpenter, S., Foley, J. A., Folke, C. and Walker, B. (2001b). Catastrophic shifts in ecosystems. *Nature*, 413(6856):591–596.

Scheffer, M., Bascompte, J., Brock, W. A., Brovkin, V., Carpenter, S. R., Dakos, V. , Held, H., van Nes, E. H., Rietkerk, M. and Sugihara, G. (2009). Early-warning signals for critical transitions. *Nature*, 461(7260):53–59.

Scheiner, S. M. (2013). The ecological literature, an idea-free distribution. *Ecology Letters*, 16(12):1421–1423.

Shoemaker, L. G., Sullivan, L. L., Donohue, I., Cabral, J. S., Williams, R. J., Mayfield, M. M., Chase, J. M., Chu, C., Harpole, W. S., Huth, A., HilleRisLambers, J., James, A. R., Kraft, N. J., May, F., Muthukrishnan, R., Satterlee, S., Taubert, F., Wang, X., Wiegand, T., Yang, Q., and Abbott, K. C. (2020). Integrating the underlying structure of stochasticity into community ecology. *Ecology*, 101(2):1–17.

Shoji, J., Toshito, S. I., Mizuno, K. I., Kamimura, Y., Hori, M., and Hirakawa, K. (2011). Possible effects of global warming on fish recruitment: Shifts in spawning season and latitudinal distribution can alter growth of fish early life stages through changes in daylength. *ICES Journal of Marine Science*, 68(6):1165–1169.

Siteur, K., Eppinga, M. B., Doelman, A., Siero, E., and Rietkerk, M. (2016). Ecosystems off track: rate-induced critical transitions in ecological models. *Oikos*, 125(12):1689–1699.

Song, H., Kemp, D. B., Tian, L., Chu, D., Song, H., and Dai, X. (2021). Thresholds of temperature change for mass extinctions. *Nature Communications*, 12(1).

Su, J. (2001). The Phenomenon of Delayed Bifurcation and its Analyses. Number 1, pages 203–214.

Tabi, A., Garnier, A. and Pennekamp, F. (2020). Testing multiple drivers of the temperature-size rule with nonlinear temperature increase. *Functional Ecology*, 34:2503–2512.

Tan, B. L. and Chia, T. T. (1996). Self-similarity and Fine Structures in the Linear-logistic Map. *Complex systems*, 10:321–344.

Tsuchiya, T. and Yamagishi, D. (1997). The Complete Bifurcation Diagram for the Logistic Map. *Zeitschrift fur Naturforschung - Section A Journal of Physical Sciences*, 52(6-7):513–516.

Turchin, P. and Ellner, S. P. (2000). Living on the edge of chaos: Population dynamics of fennoscandian voles. *Ecology*, 81(11):3099–3116.

1049 Turchin, P., Taylor, A. D., and Reeve, J. D. (1999). Dynamical role of predators in population
1050 cycles of a forest insect: An experimental test. *Science*, 285(5430):1068–1071.

1051 Van De Pol, M., Vindenes, Y., Sæther, B. E., Engen, S., Ens, B. J., Oosterbeek, K., and Tinbergen,
1052 J. M. (2010). Effects of climate change and variability on population dynamics in a long-lived
1053 shorebird. *Ecology*, 91(4):1192–1204.

1054 van der Wiel, K. and Bintanja, R. (2021). Contribution of climatic changes in mean and
1055 variability to monthly temperature and precipitation extremes. *Communications Earth and*
1056 *Environment*, 2(1):1–11.

1057 Vanselow, A., Halekotte, L., and Feudel, U. (2022). Evolutionary rescue can prevent rate-induced
1058 tipping. *Theoretical Ecology*, 15(1):29–50.

1059 Vanselow, A., Wieczorek, S., and Feudel, U. (2019). When very slow is too fast - collapse of a
1060 predator-prey system. *Journal of Theoretical Biology*, 479:64–72.

1061 Vitousek, P. M. (1994). Beyond Global Warming: Ecology and Global Change. *Ecology*,
1062 75(7):1861–1876.

1063 Walther, G. R., Post, E., Convey, P., Menzel, A., Parmesan, C., Beebee, T. J., Fromentin, J. M.,
1064 Hoegh-Guldberg, O., and Bairlein, F. (2002). Ecological responses to recent climate change.
1065 *Nature*, 416(6879):389–395.

1066 Wei, H. M., Li, X. Z., and Martcheva, M. (2008). An epidemic model of a vector-borne disease
1067 with direct transmission and time delay. *Journal of Mathematical Analysis and Applications*,
1068 342(2):895–908.

1069 Williams, J. W., Ordonez, A., and Svenning, J. C. (2021). A unifying framework for studying and
1070 managing climate-driven rates of ecological change. *Nature Ecology and Evolution*,
1071 5(1):17–26.

Wrzosek, D. M. (1990). Limit cycles in predator-prey models. *Mathematical Biosciences*, 98(1):1–12.

Wu, X. P. and Wang, L. (2017). Zero-Hopf bifurcation analysis in delayed differential equations with two delays. *Journal of the Franklin Institute*, 354(3):1484–1513.

Zarada, K. and Drake, J. M. (2017). Time to extinction in deteriorating environments. *Theoretical Ecology*, 10(1):65–71.

Box 1: Glossary

time-varying demographic parameter: demographic rate (e.g. survival) that varies with the environment and therefore over time. Its time series accounts for both the time-series of environmental cues and the response of the demographic rate to these cues.

Stationary environment: environmental framework where demographic rates vary over time, but their long-term statistical properties (e.g., mean, variance) are constant.

Environmental trend: (non-stationary) environmental framework where one (or more) demographic rate(s) increases or decreases consistently over time.

Environmental rate of change (r): the speed at which a given demographic rate changes over time.

Regime shift: a qualitative change in the dynamics of a population, or the dynamics and/or composition of a community.

Tipping point: critical threshold that, when crossed, leads to a sudden, quantitative and qualitative change in population dynamics. For a b**-tipping point**, this threshold corresponds to a certain, value of the focal demographic rate. For a r**-tipping point**, it corresponds to a certain value of a the environmental rate of change.

Bifurcation: a certain value of a demographic rate separating, in a constant environment, qualitatively different long-term (asymptotic) dynamics. The **bifurcation diagram** provides the asymptotic dynamics for a continuum of values of the demographic rate. For **discontinuous bifurcations**, there is no (positive) equilibrium point on one side of the bifurcation (e.g., fold or saddle-node bifurcations).

Equilibrium: in a constant environment, the state of a system where dynamics have become constant over time (e.g., constant abundances or generation cycles of constant period and amplitudes). If a small perturbation away from the equilibrium leads back to it, the equilibrium is deemed **stable** (i.e., an **attractor**). An equilibrium can correspond to a single abundance value (**point equilibrium**) or a series of values (**cycle**) that asymptotic abundances encounter with fixed period.

Chaotic range: range of values of the demographic rate where the asymptotic dynamics are chaotic (i.e., no stable attractor).

Moving equilibrium: abundance point, corresponding to an equilibrium in a constant environment, that changes over time due to environmentally driven changes in a demographic parameter (see eq.4). **Ghost attractor**: In the context of this study, a ghost attractor is, in a varying environment, a state of the system that would be an equilibrium (stable or unstable) if demographic rates were held constant. More generally, it is "a state that is not an equilibrium, but would be under slightly different conditions" (Hastings et al., 2018).

Transients: transient dynamics correspond to the trajectory of a system towards the asymptotic regime, following an instantaneous perturbation, or initiation of the population away from the asymptotic attractor. In some cases, called **long transients** these regimes can last for many generations and incur sudden changes in abundances occurring long after the perturbation. **Under-compensatory**, respectively **over-compensatory**, transients correspond to transient dynamics where the equilibrium is reached via monotonic – constantly increasing or decreasing – changes in abundance, respectively via (damped) oscillating abundances (abundances overcompensate).

Superimposition diagram: superimposition of the bifurcation diagram with the abundance dynamics considered in the alternative timescale of the demographic rate.

r-bifurcation diagram: Properties of population dynamics (e.g., bifurcation or post-trend transient) displayed for a continuum of values of the rate of environmental change.

List of Figures

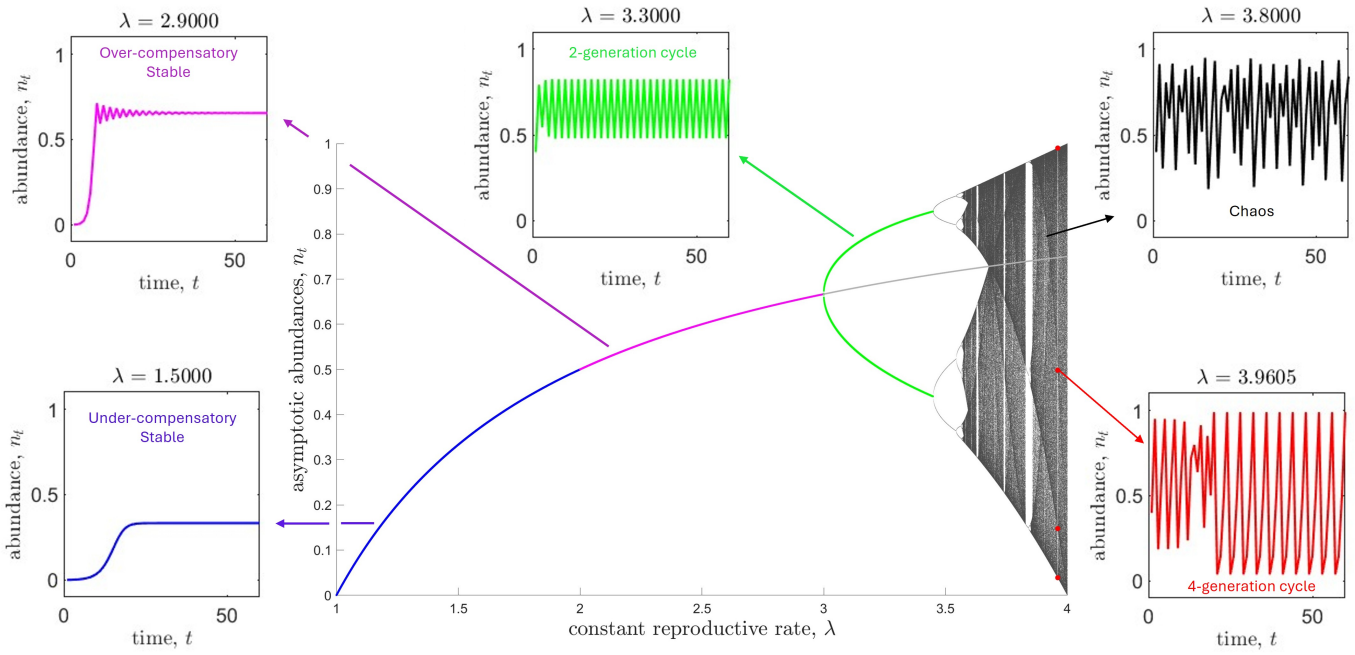
λ = 2.9000
Over-compensatory
Stable
abundance, n_t
time, t
λ = 3.3000
2-generation cycle
λ = 3.8000
Chaos
λ = 1.5000
Under-compensatory
Stable
λ = 3.9605
4-generation cycle
asymptotic abundances, n_t
constant reproductive rate, λ

Figure 1

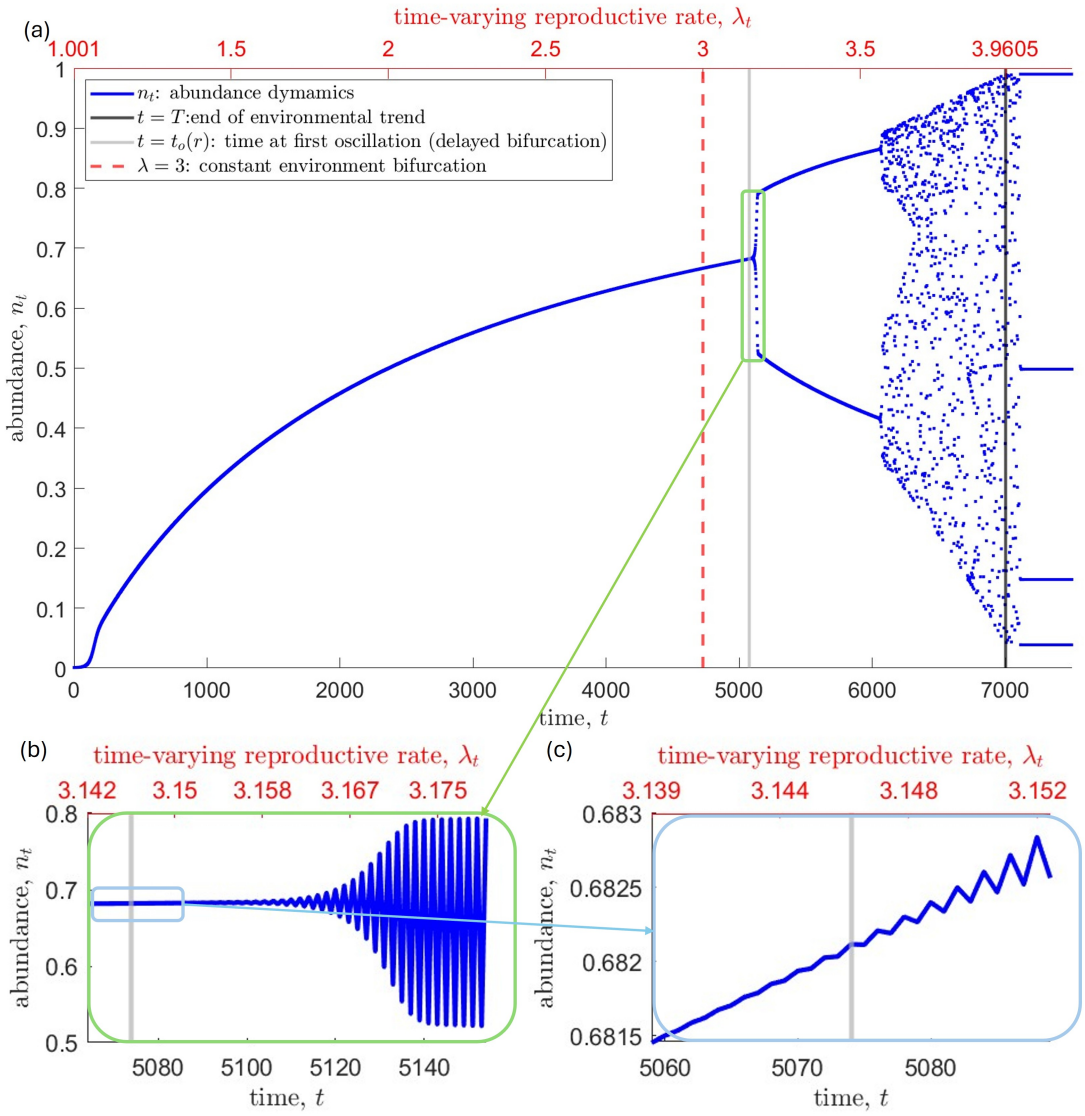
(a)
time-varying reproductive rate, λ_t
1.001
1.5
2
2.5
3
3.5
3.9605
n_t: abundance dymamics
$t = T$:end of environmental trend
$t = t_o(r)$: time at first oscillation (delayed bifurcation)
$\lambda = 3$: constant environment bifurcation
abundance, n_t
time, t
(b)
time-varying reproductive rate, λ_t
3.142
3.15
3.158
3.167
3.175
abundance, n_t
time, t
(c)
time-varying reproductive rate, λ_t
3.139
3.144
3.148
3.152
abundance, n_t
time, t

Figure 2

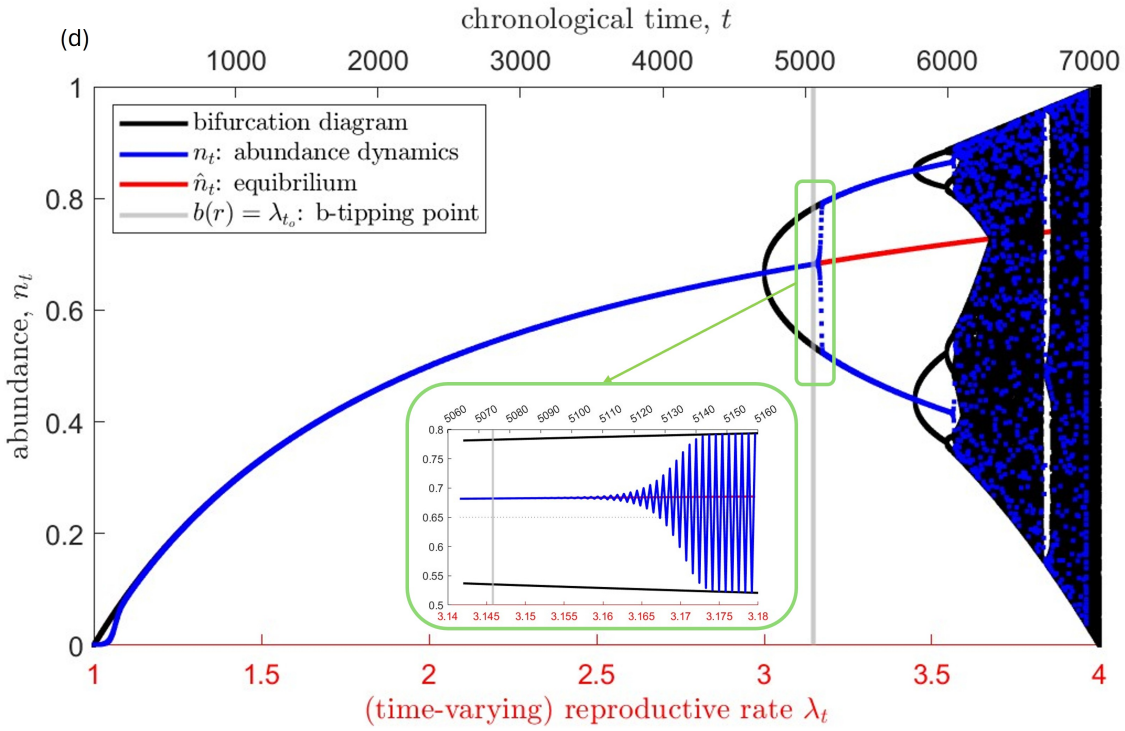
(d)
chronological time, t
1000
2000
3000
4000
5000
6000
7000
bifurcation diagram
n_t: abundance dynamics
$\hat{n}_t$: equibrilium
$b(r) = \lambda_{t_o}$: b-tipping point
abundance, n_t
0
0.2
0.4
0.6
0.8
1
1
1.5
2
2.5
3
3.5
4
(time-varying) reproductive rate λ_t
5060
5070
5080
5090
5100
5110
5120
5130
5140
5150
5160
0.8
0.75
0.7
0.65
0.6
0.55
0.5
3.14
3.145
3.15
3.155
3.16
3.165
3.17
3.175
3.18

Figure 3

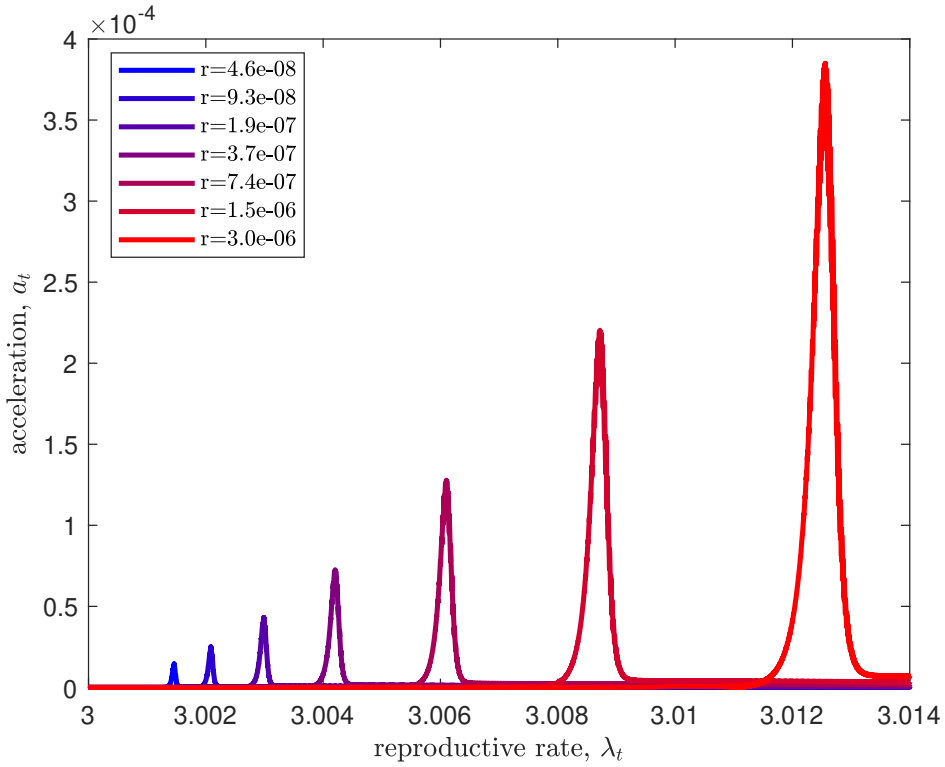
×10^-4
4
3.5
3
2.5
2
1.5
1
0.5
0
r=4.6e-08
r=9.3e-08
r=1.9e-07
r=3.7e-07
r=7.4e-07
r=1.5e-06
r=3.0e-06
acceleration, a_t
3
3.002
3.004
3.006
3.008
3.01
3.012
3.014
reproductive rate, λ_t

Figure 4

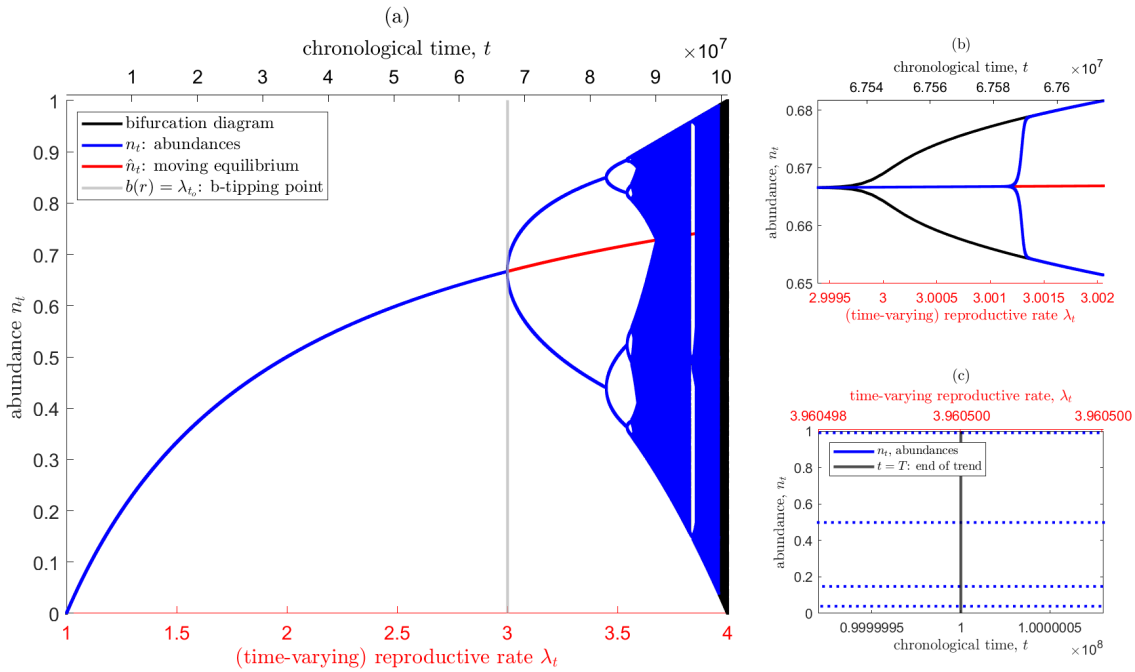
(a)
chronological time, t
$\times 10^7$
bifurcation diagram
n_t: abundances
$\hat{n}_t$: moving equilibrium
$b(r) = \lambda_{t_o}$: b-tipping point
abundance n_t
(time-varying) reproductive rate λ_t
(b)
chronological time, t
$\times 10^7$
abundance, n_t
(time-varying) reproductive rate λ_t
(c)
time-varying reproductive rate, λ_t
n_t, abundances
$t = T$: end of trend
abundance, n_t
chronological time, t
$\times 10^8$

Figure 5

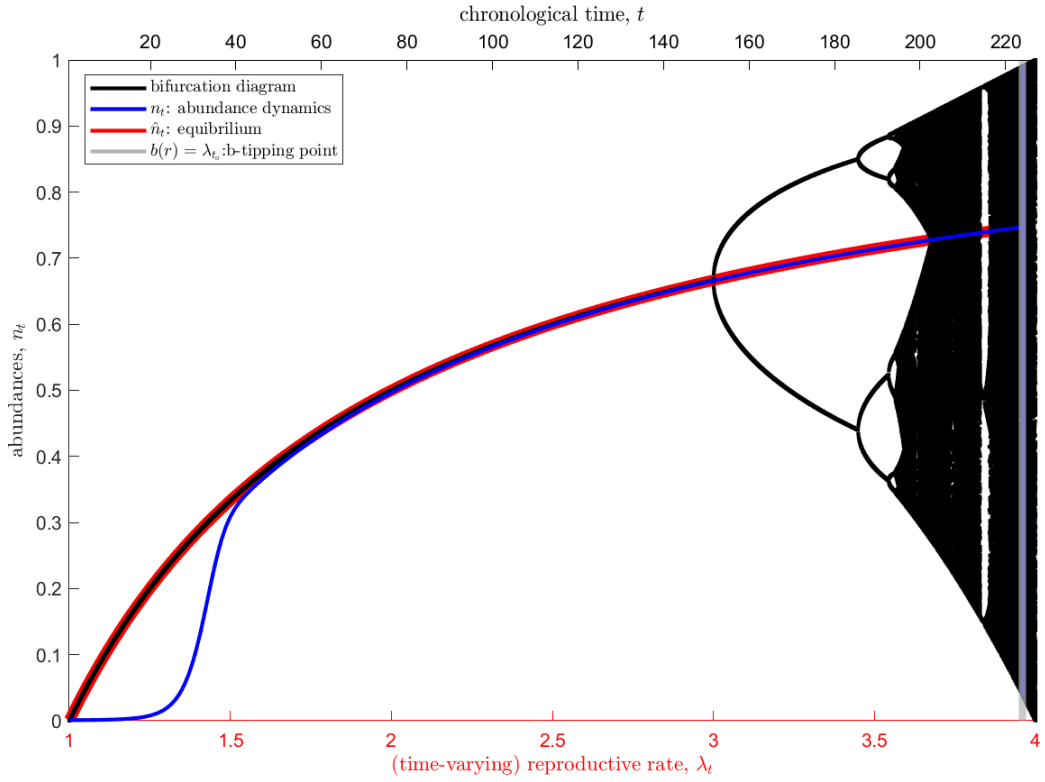
chronological time, t
20
40
60
80
100
120
140
160
180
200
220
bifurcation diagram
n_t: abundance dynamics
$\hat{n}_t$: equibrilium
$b(r) = \lambda_{t_c}$:b-tipping point
abundances, n_t
0
0.1
0.2
0.3
0.4
0.5
0.6
0.7
0.8
0.9
1
1
1.5
2
2.5
3
3.5
4
(time-varying) reproductive rate, λ_t

Figure 6

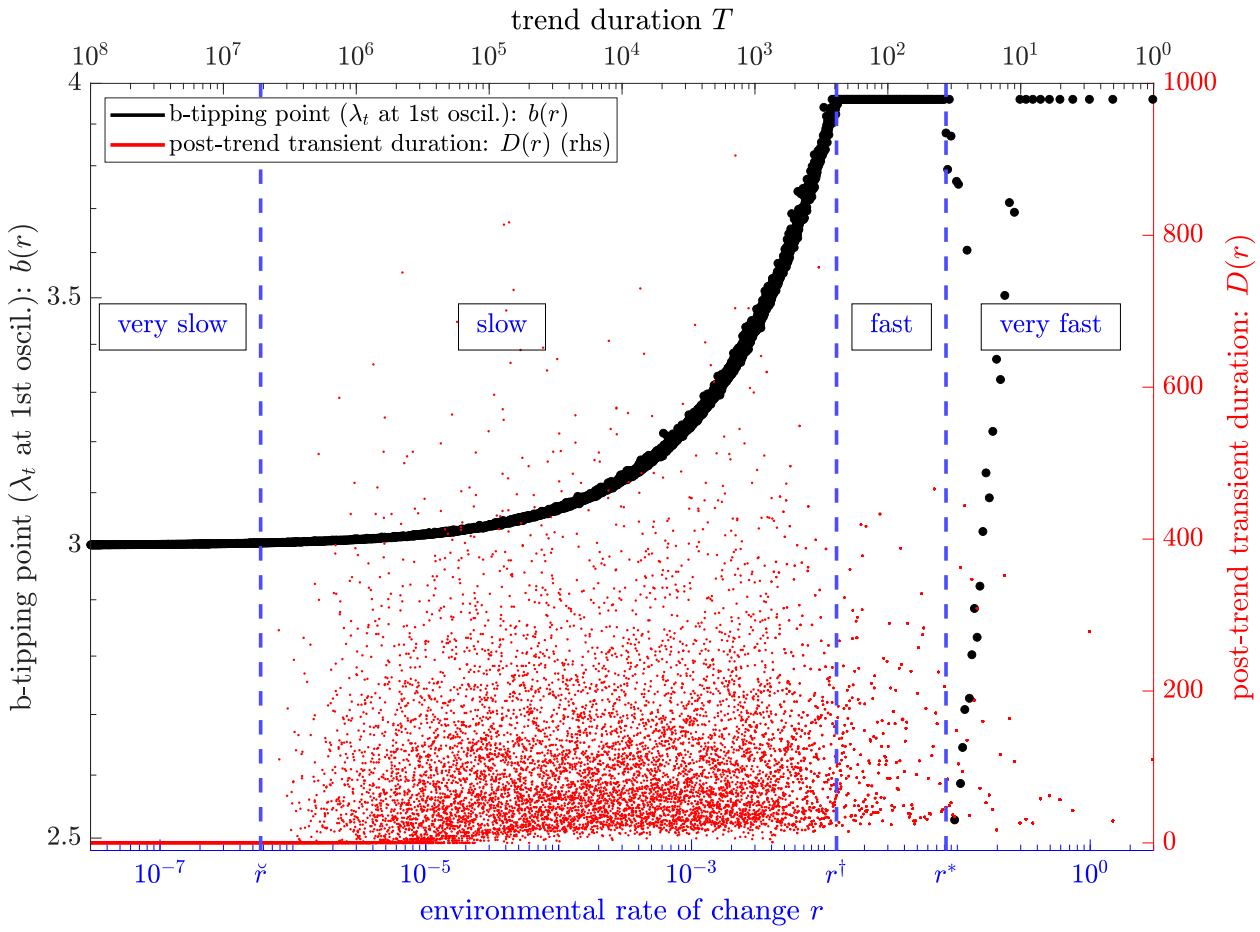
trend duration T
10^8
10^7
10^6
10^5
10^4
10^3
10^2
10^1
10^0
b-tipping point (λ_t at 1st oscil.): $b(r)$
post-trend transient duration: $D(r)$ (rhs)
very slow
slow
fast
very fast
b-tipping point (λ_t at 1st oscil.): $b(r)$
post-trend transient duration: $D(r)$
4
3.5
3
2.5
1000
800
600
400
200
0
10^{-7}
$\breve{r}$
10^{-5}
10^{-3}
$r^\dagger$
r^*
10^0
environmental rate of change r

Figure 7

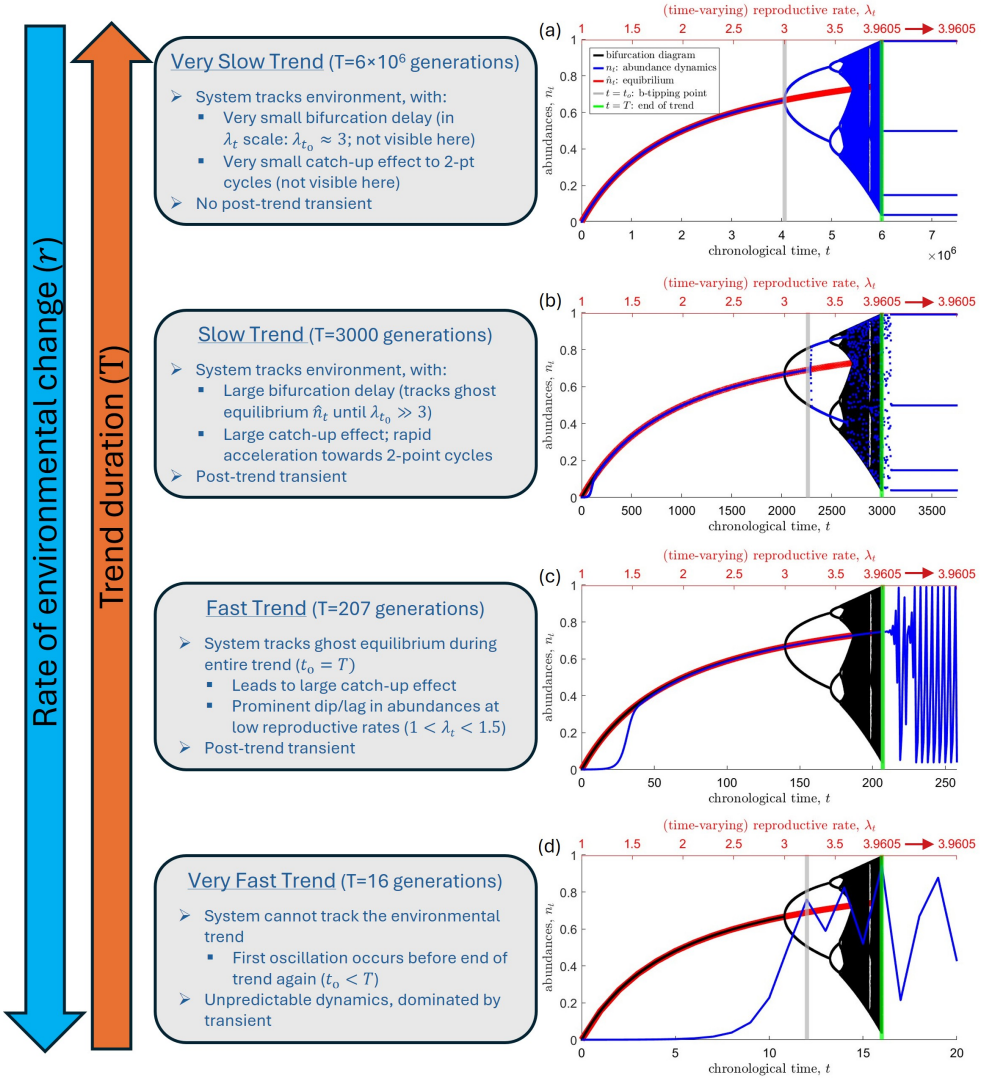
Rate of environmental change (r)
Trend duration (T)
Very Slow Trend (T=6×10^6 generations)
System tracks environment, with:
Very small bifurcation delay (in λ_t scale: λ_{t_0} ≈ 3; not visible here)
Very small catch-up effect to 2-pt cycles (not visible here)
No post-trend transient
Slow Trend (T=3000 generations)
System tracks environment, with:
Large bifurcation delay (tracks ghost equilibrium n̂_t until λ_{t_0} ≫ 3)
Large catch-up effect; rapid acceleration towards 2-point cycles
Post-trend transient
Fast Trend (T=207 generations)
System tracks ghost equilibrium during entire trend (t_0 = T)
Leads to large catch-up effect
Prominent dip/lag in abundances at low reproductive rates (1 < λ_t < 1.5)
Post-trend transient
Very Fast Trend (T=16 generations)
System cannot track the environmental trend
First oscillation occurs before end of trend again (t_0 < T)
Unpredictable dynamics, dominated by transient
(a)
(b)
(c)
(d)
(time-varying) reproductive rate, λ_t
1 1.5 2 2.5 3 3.5 3.9605 → 3.9605
bifurcation diagram
n_t: abundance dynamics
n̂_t: equilibrium
t = t_0: b-tipping point
t = T: end of trend
abundances, n_t
chronological time, t
×10^6

Figure 8

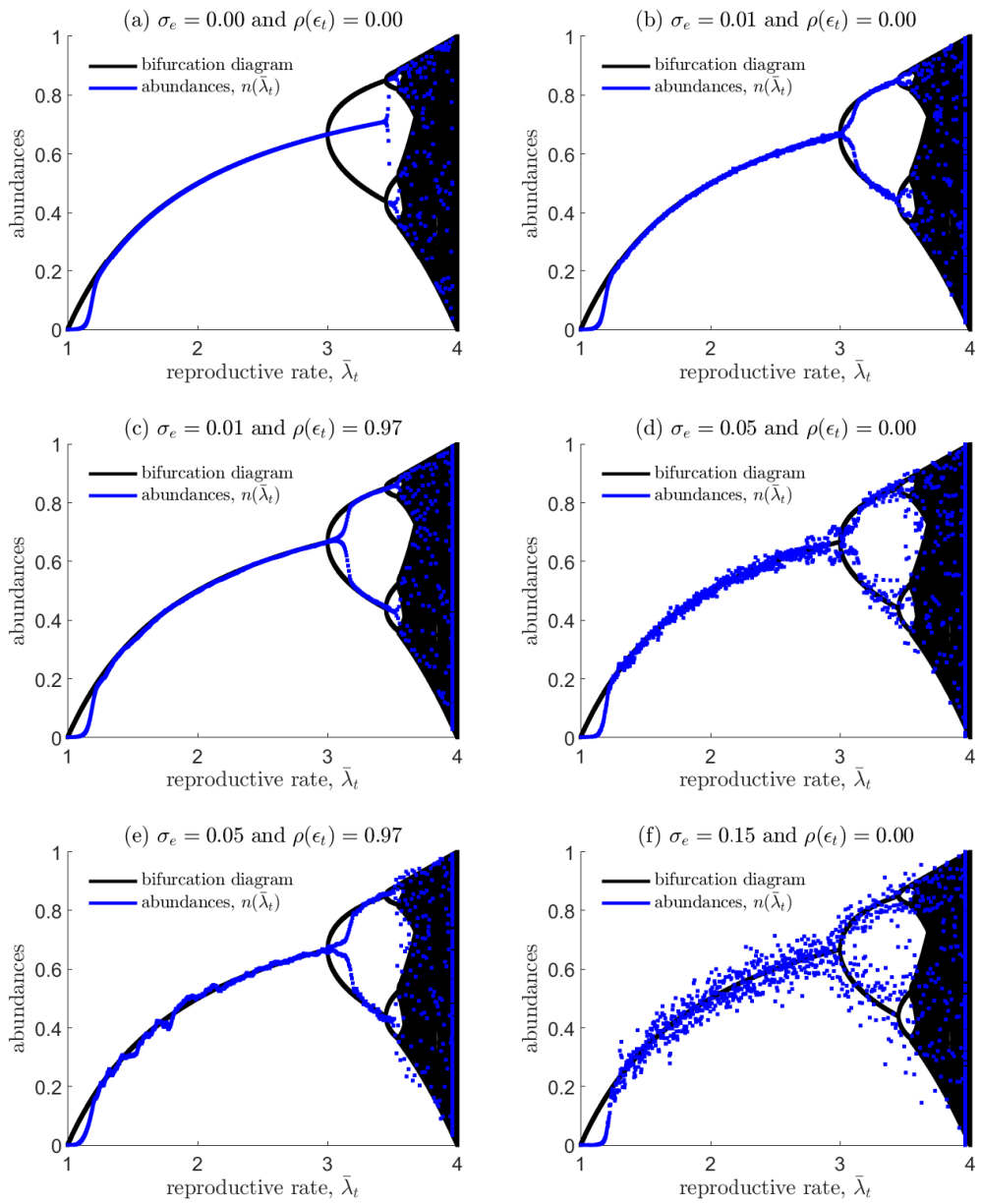
(a) $\sigma_e = 0.00$ and $\rho(\epsilon_t) = 0.00$
(b) $\sigma_e = 0.01$ and $\rho(\epsilon_t) = 0.00$
(c) $\sigma_e = 0.01$ and $\rho(\epsilon_t) = 0.97$
(d) $\sigma_e = 0.05$ and $\rho(\epsilon_t) = 0.00$
(e) $\sigma_e = 0.05$ and $\rho(\epsilon_t) = 0.97$
(f) $\sigma_e = 0.15$ and $\rho(\epsilon_t) = 0.00$
bifurcation diagram
abundances, $n(\bar{\lambda}_t)$
abundances
reproductive rate, $\bar{\lambda}_t$
0
0.2
0.4
0.6
0.8
1
1
2
3
4

Figure 9

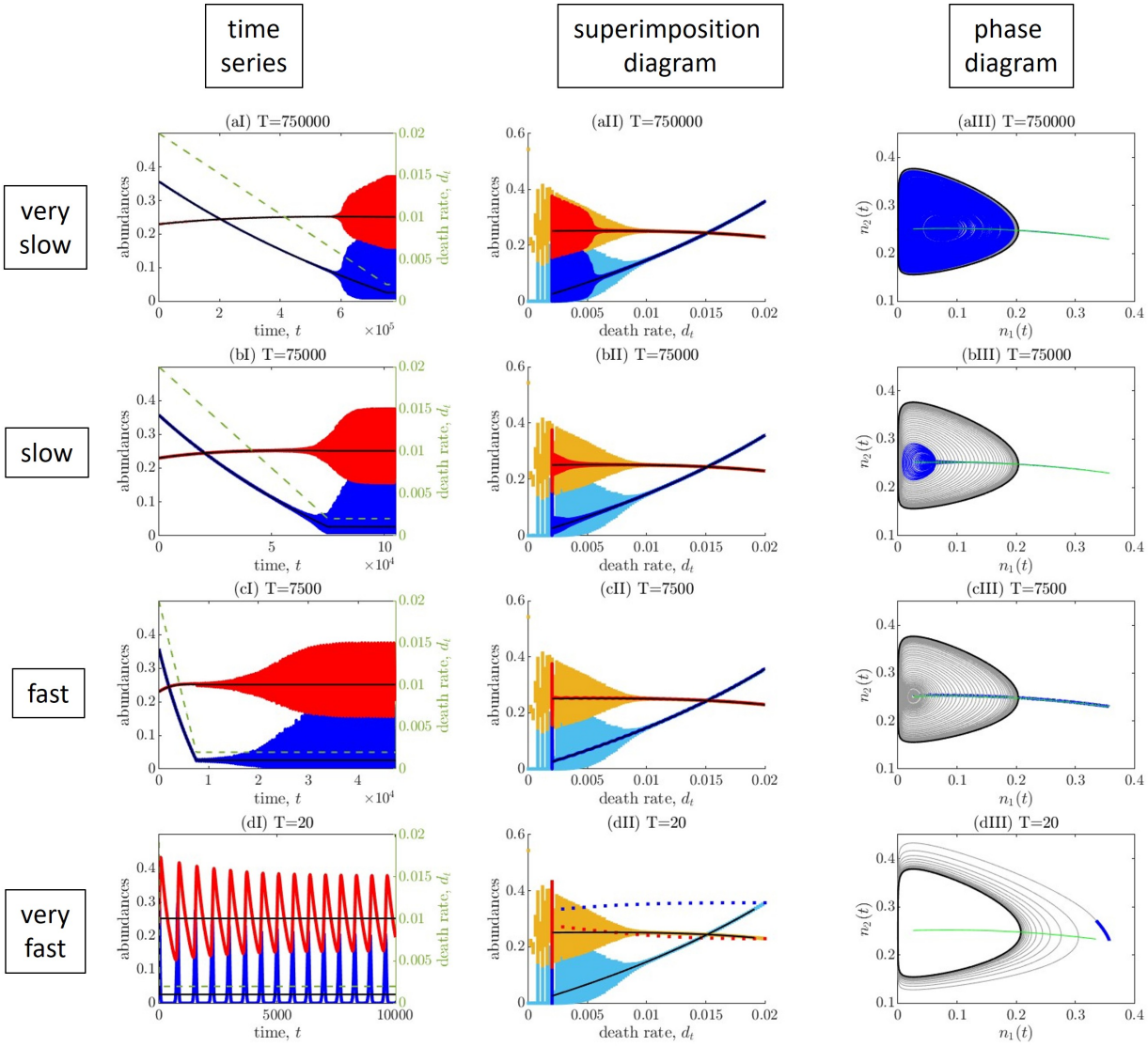
time series
superimposition diagram
phase diagram
very slow
slow
fast
very fast
(aI) T=750000
(aII) T=750000
(aIII) T=750000
(bI) T=75000
(bII) T=75000
(bIII) T=75000
(cI) T=7500
(cII) T=7500
(cIII) T=7500
(dI) T=20
(dII) T=20
(dIII) T=20
abundances
death rate, d_t
time, t
$\times 10^5$
$\times 10^4$
$n_1(t)$
$n_2(t)$

Figure 10

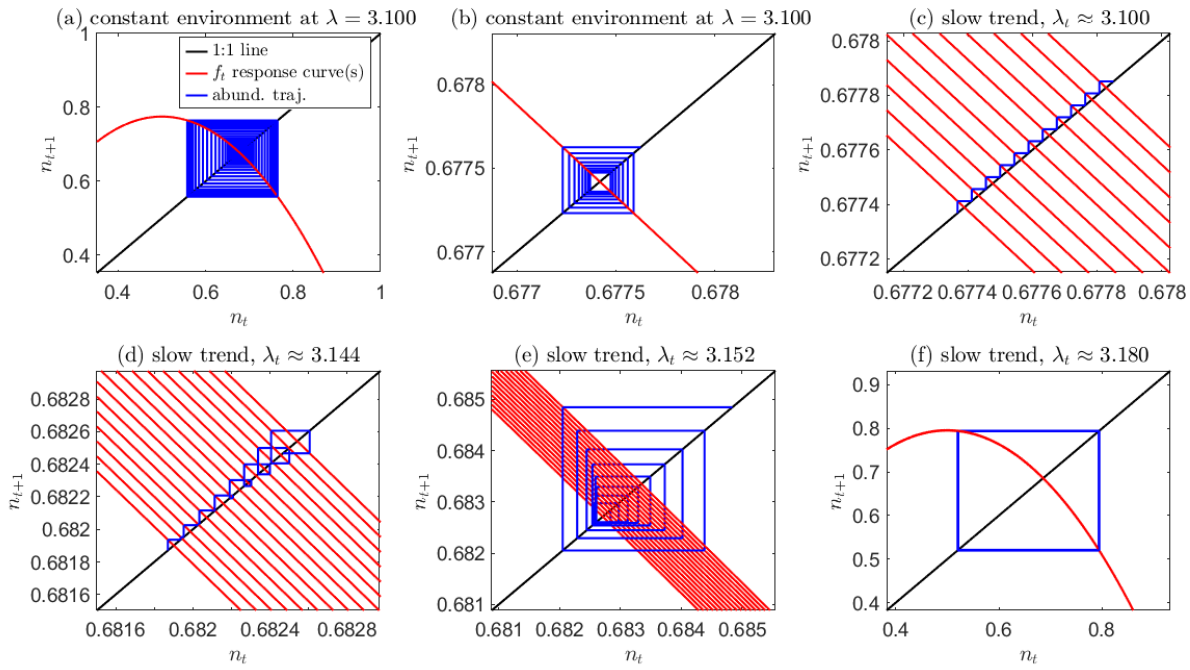
(a) constant environment at $\lambda = 3.100$
1:1 line
f_t response curve(s)
abund. traj.
(b) constant environment at $\lambda = 3.100$
(c) slow trend, $\lambda_t \approx 3.100$
(d) slow trend, $\lambda_t \approx 3.144$
(e) slow trend, $\lambda_t \approx 3.152$
(f) slow trend, $\lambda_t \approx 3.180$
n_{t+1}
n_t

Figure 11

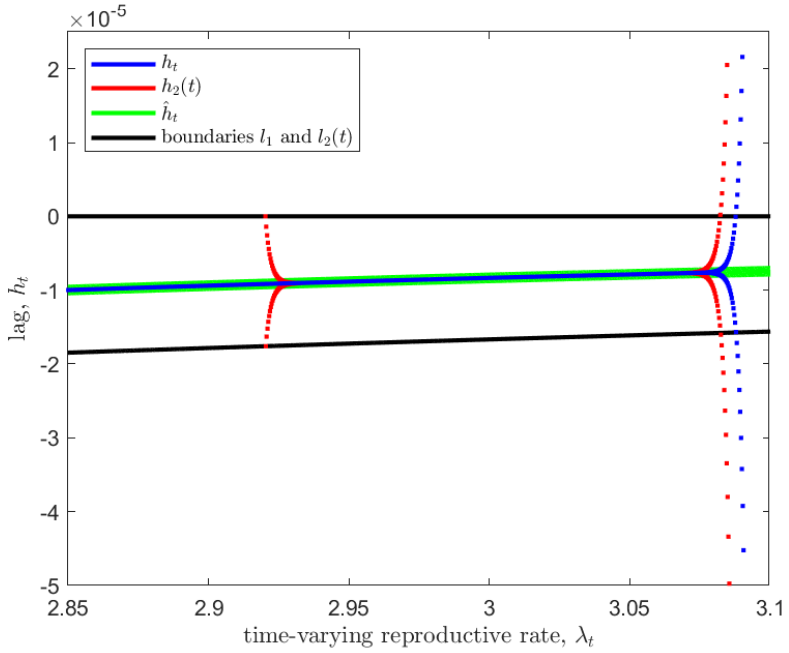
×10^-5
2
1
0
-1
-2
-3
-4
-5
2.85
2.9
2.95
3
3.05
3.1
h_t
$h_2(t)$
$\hat{h}_t$
boundaries l_1 and $l_2(t)$
lag, h_t
time-varying reproductive rate, λ_t

Figure 12

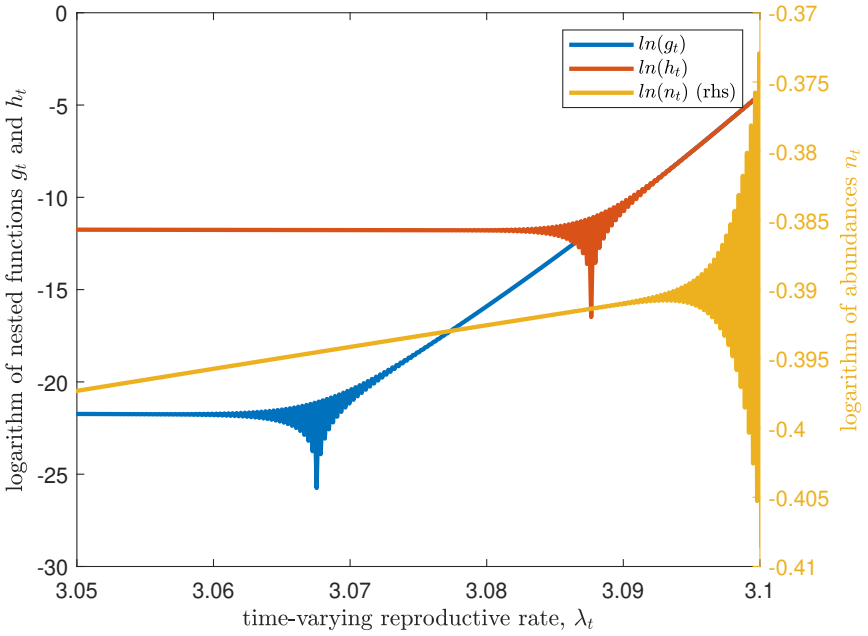
0
-5
-10
-15
-20
-25
-30
3.05
3.06
3.07
3.08
3.09
3.1
-0.37
-0.375
-0.38
-0.385
-0.39
-0.395
-0.4
-0.405
-0.41
$ln(g_t)$
$ln(h_t)$
$ln(n_t)$ (rhs)
logarithm of nested functions g_t and h_t
logarithm of abundances n_t
time-varying reproductive rate, λ_t

Figure 13

Appendix S1

A1 Dynamics of the logistic map in constant environments

In a constant environment, the asymptotic behaviour of a population following the logistic map ($n_{t+1} = \lambda n_t\,(1 - n_t)$; eq. 1) is determined by the value of the parameter λ, the reproductive rate in the absence of intraspecific competition. Qualitative differences in population dynamics can be

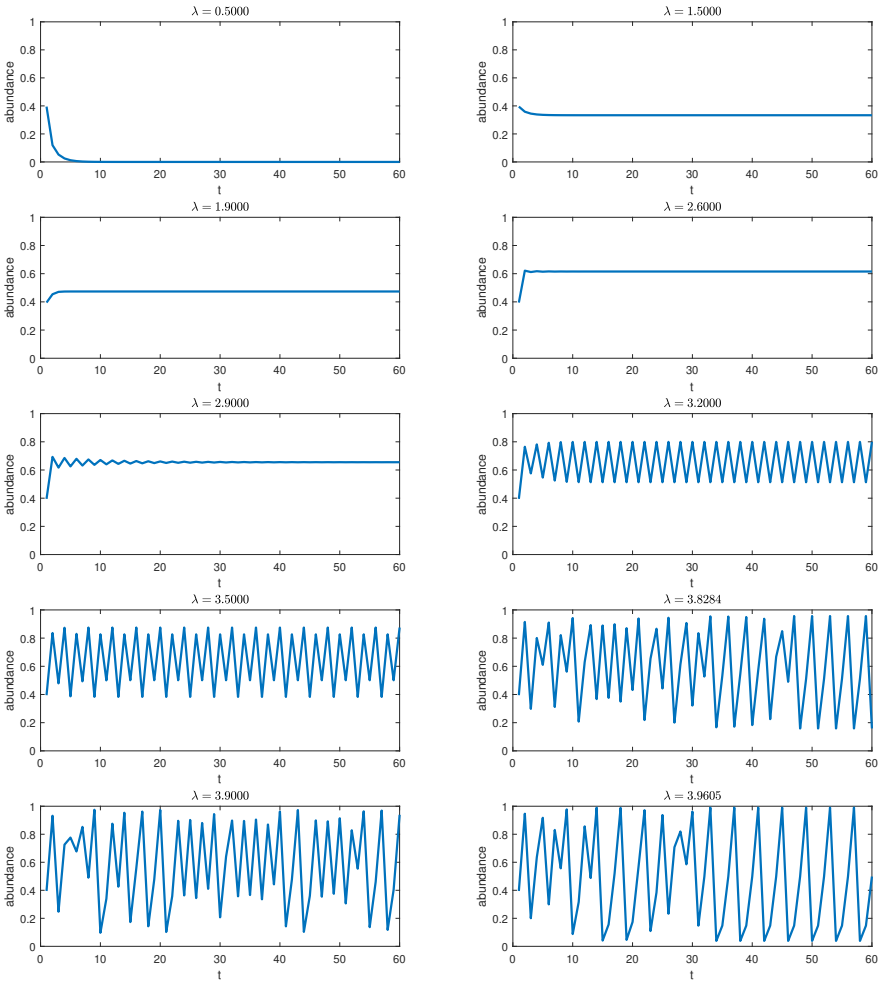

Figure S1: Transient and asymptotic dynamics of the logistic map (eq.1) for $n_0 = 0.395$ and various values of λ. For $\lambda < 1$, the abundance converges towards 0. For $1 < \lambda < 3$, abundances converge towards $\hat{n} = 1 - \frac{1}{\lambda}$, with damped (overcompensatory) oscillations for $\lambda > 2$ ($J(\hat{n}) < 0$) but no oscillations for $\lambda < 2$ ($J(\hat{n}) > 0$). The equilibrium is unstable for $\lambda > 3$ ($J(\hat{n}) < -1$), which is a period doubling bifurcation ($\lambda = 3.2$ generates a 2-generation asymptotic cycle), followed by others (for $\lambda = 3.5$ we have a 4-generation asymptotic cycle) until $\lambda \approx 3.54409$ which is the onset of chaos (e.g., for $\lambda = 3.9$). Above that, the behaviour will be chaotic for most values of λ, but there are still certain "islands of periodic stability" or "periodic windows" such as $\lambda = 3.828$ which exhibits a 3-generation asymptotic cycle and $\lambda = 3.9605 = \lambda_T$ which exhibits a 4-generation asymptotic cycle.

understood from the *Jacobian*, which corresponds, for unstructured models like the logistic map, to the derivative of the population growth function $J = \frac{df}{dn}$ following an arbitrarily small perturbation, evaluated at the non-trivial equilibrium: $J(\hat{n}) = 2 - \lambda$. As long as $-1 < J(\hat{n}) < 1$, the population will return to the equilibrium following a small perturbation, which maps onto the stable equilibrium region $1 < \lambda < 3$ in fig.1. However the trajectory to the equilibrium will differ qualitatively according to the sign of $J(\hat{n})$. When $1 < \lambda < 2$, $J(\hat{n}) > 0$, the stable equilibrium is approached monotonically (i.e., smoothly; under-compensation), while for $2 < \lambda < 3$, $J(\hat{n}) < 0$, the population trajectory shows damped oscillations (over-compensation). This distinction is crucial for transient regimes, as well as when studying environments that fluctuate around a fixed mean value (Nisbet and Gurney, 1985; Greenman and Benton, 2003). As λ approaches 3 from below, the 2-generation auto-correlation of the noisy (but stationary) version of the logistic map approaches -1 (see SMA3): the population displays quasi 2-generation cycles, that is, noisy oscillations between consecutive low- and high abundances that appear similar to a deterministic 2-generation cycle. The sign and the amplitude of the Jacobian therefore provides useful information for small deviations from the equilibrium and for certain equilibria, but is not generally sufficient to understand the road to the asymptotic behaviour. Fig.S1 shows the transient and asymptotic population dynamics for representative values of λ, for a given arbitrary initial population abundance, $n_0 = 0.395$.

Periods of the generation cycles of the logistic map

The bifurcation diagram (fig.1) provides valuable information about the existence and range of stable point equilibria, as well as the appearance of period-doubling bifurcations and the amplitude of asymptotic cycles or chaotic bounds. However, the exact onset of chaos and the "islands of periodic stability" that occur after that onset are less easy to spot on the bifurcation diagram (without zooming in on narrower parameter ranges). Instead, one can compute the Lyapunov exponent or directly compute the period of an asymptotic cycle (if it exists). For a range of λ values and for arbitrary initial condition $n_0 = 0.1$, we produce the abundance dynamics for

the logistic map across $1,000$ generations and compute the Lyapunov exponent of the abundance time-series (in red on fig.S2, right-hand scale). The Lyapunov exponent is negative for periodic cycles and positive for chaotic dynamics. To compute the period of the cycles, we simulate dynamics across $40,000$ generations and focus on the last 700 generations. We test whether $max_t(n(t+j) - n(t))^2 < \epsilon$, for $\epsilon = 10^{-5}$, for increasing values of j starting at 1. For each value of the parameter λ, we allocate the first value of j for which the condition is respected as its "cycle period". When, by $j = 100$, no cycle has been found, we allocate a "cycle period" of -1, which we call chaos (but it can also correspond to a cycle of period > 100 generations, or a shorter cycle period with an extremely long, *supertransient*). We display these "cycle periods" in blue on fig.S2; where we only focus on periods between 1 and 7, and allocate "cycle period" 0 to periodic cycles of period comprised between 8 and 100. This allows to identify the highest values of λ for which one has an asymptotic cycle of period <8: it is a 4-generation range (highlighted with an orange circle in fig.S2), comprising $\lambda_T = 3.9605$.

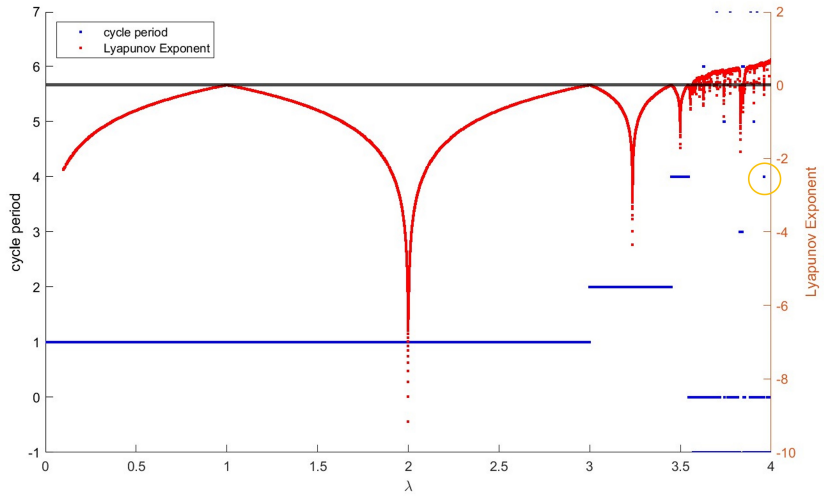

Figure S2: cycle period (blue) and Lyapunov Exponent (red, rhs) for the logistic map (eq.1). Period -1 indicates chaos (or cycles of period>100) and period 0 indicate a cyclic behaviour with 7 < period < 100.

Transient dynamics for a window of periodic stability: $\lambda = \lambda_T = 3.9605$

Focusing, in particular, on $\lambda = \lambda_T = 3.9605$, leading to an asymptotic 4-generation cycle for any initial condition, we want to understand how the initial conditions (n_0) affect the transient towards the 4-generation cycle and its duration. For $n_0 = \hat{n}(\lambda_0) \approx 0.001$, this corresponds to the step-change, and the dynamics are displayed in fig.S6 (bottom row): the transient is roughly 80 generations (relatively long). Here we illustrate how sensitive the transient period is to initial conditions by considering three further examples: an extremely short transient of 4-5 generations when $n_0 = 0.002$, which corresponds to an initial condition for λ_t of $\lambda_0 = 1.002$, (fig.S4, top row); the complete lack of any transient when $n_0 = 0.0387$ (which is the equilibrium for $\lambda_0 = 1.0403$, and the lowest of the four abundances of the asymptotic cycle at λ_T, fig.S4, middle row); and finally a very long transient of around 320 generations at $n_0 = 0.0377$ ($\lambda_0 = 1.0392$ fig.S4, bottom row).

We note that this model is so sensitive to initial conditions that the precise transient period can be sensitive to the numerical precision of the software used to simulate the system. Extending this analysis for a wider range of values of n_0, for which we estimate the duration of the transient via $min(t, max_t|n(t+4) - n(t)| < \epsilon)$, for $\epsilon = 0.0001$, we plot the output in fig.S3, which shows that

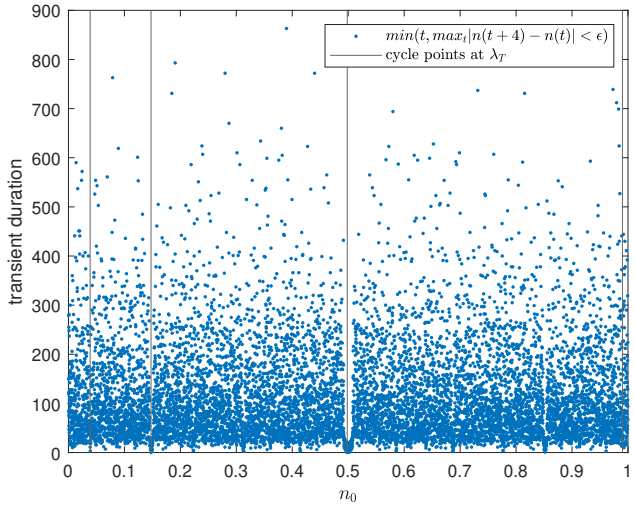

Figure S3: Transient duration for a step-change towards the logistic map of parameter $\lambda = \lambda_T = 3.9605$ (where the four points of the asymptotic cycle are represented as black vertical lines) for various initial values n_0, calculated as $min(t, max_t|n(t+4) - n(t)| < \epsilon)$, for $\epsilon = 0.0001$.

for the chosen asymptotic state corresponding to $\lambda = \lambda_T$, as a function of the choice of n_0, one can encounter transients as long as 850 generations.

A2 Bifurcation at $\lambda = 3$ and b-tipping point

In the constant environmental framework, there is a period-doubling bifurcation at $\lambda = 3$ that segregates the fixed point, non-zero equilibrium regime ($1 < \lambda < 3$) and a 2-generation cycles regime ($\lambda > 3$); see fig.1. The $\lambda = 3$ case is a neutrally stable 2-point cycle, i.e., the steady-state cycle amplitude depends on n_0. Contrary to a saddle node bifurcation – where on one side of the bifurcation there is no equilibrium point – $\lim_{r\to 0} b(r) = 3$ (which we denote $b(0)$ for simplicity) does not correspond to a discontinuity in the abundances over time. Equating the very slow trend framework with the constant environment framework, implies considering that as the rate of environmental change $r \to 0$, n_t corresponds to the asymptotic abundance of the bifurcation diagram. Fig.4, shows the "acceleration" of population change time-series, $a_t = ||n_{t+1} - n_t| - |n_t - n_{t-1}||$ in the λ_t time-scale for various rates of environmental change (r),. The acceleration peaks later ($b(r)$ increases with r) and higher as the rate of environmental change r increases. Fig.S5 displays the value of the delay in the bifurcation $b(r)$ (red, rhs) and $d(r) = max_t(a_t)$, the peak in acceleration, , as a function of r; a metric for the discontinuity generated in abundance time series. As $r \to 0$, $b(r) \to b(0) = 3$ and $d(r) \to 0$: there is no regime shift or discontinuity, for a paradoxical trend with speed $r = 0$. However, for any "real" positive trend, $r > 0$, there is a discontinuity as λ_t passes $b(r)$ – measured by $d(r) = max(|n_{t+1} - n_t| - |n_t - n_{t-1}|)$ – that increases in magnitude as r increases (figs 4,S5 and S6). In other words, the trend turns a simple, continuous, bifurcation into a tipping point at $b(r) \quad \forall \quad 0 < r < t_r$. In summary, $b(r)$ is not a b-tipping point for a (paradoxical) trend of speed $r = 0$, but one for any real trend $r > 0$ (see SMA2).

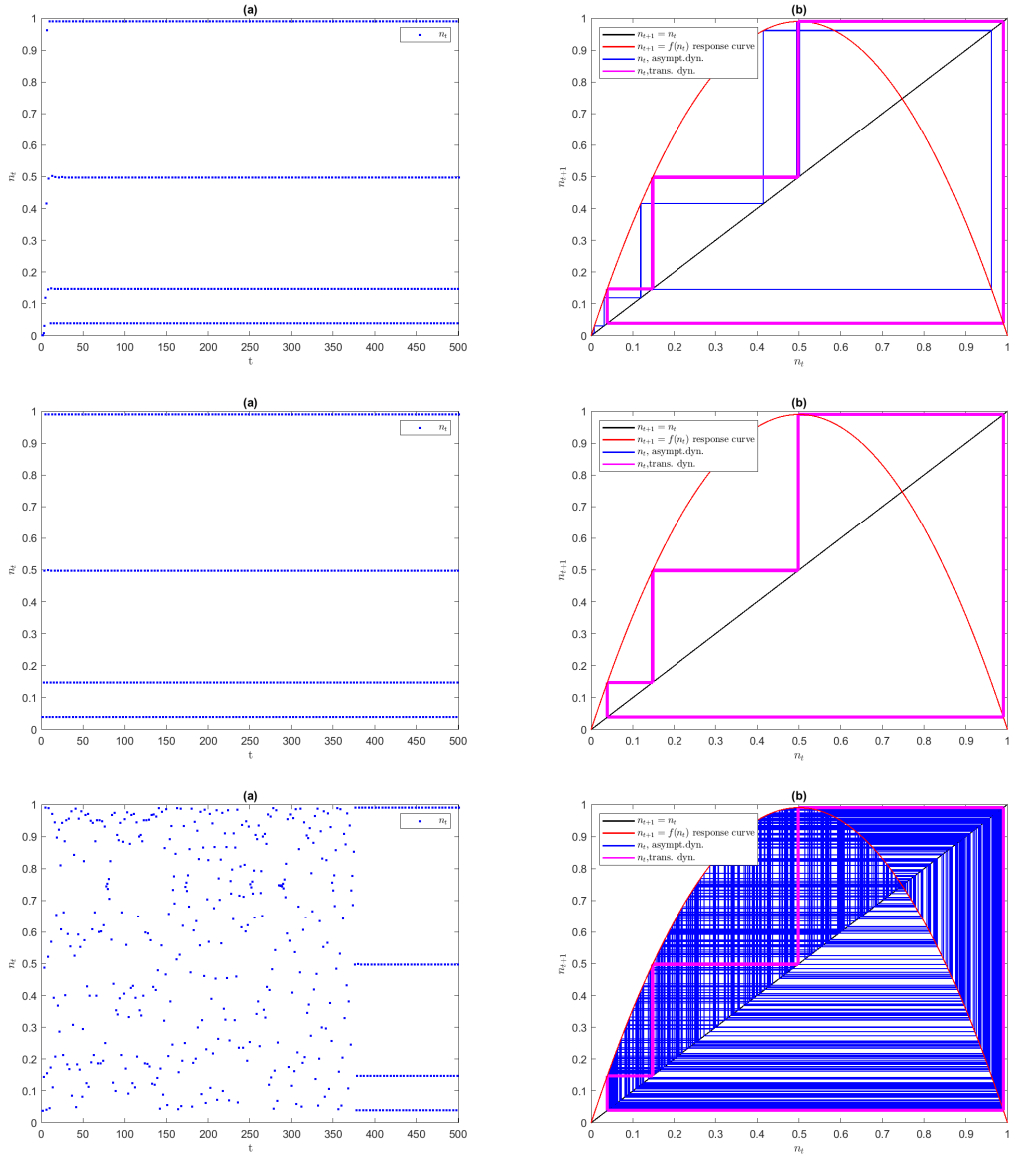

Figure S4: Sensitivity of transient period to initial conditions; trends dynamics of a step change (T=1) from λ_0 (and $n_0 = \hat{n}(\lambda_0)$) to $\lambda_T = 3.9605$, followed by 500 generations at the constant environment; (a) left panels: abundance n_t (blue) and environmental parameter λ_t (red, secondary axis); (b) right panels cobweb diagram: response curve (in red) and the abundance trajectory (in blue, transient, in pink, asymptotic). (top) $\lambda_0 = 1.002$: extremely short transient dynamics (4 generations) ,(middle) $\lambda_0 = 1.0403$ complete lack of transient dynamics; $\lambda_T = 3.9605$ (bottom) $\lambda_0 = 1.0392$ very long transient dynamics (320 generations).

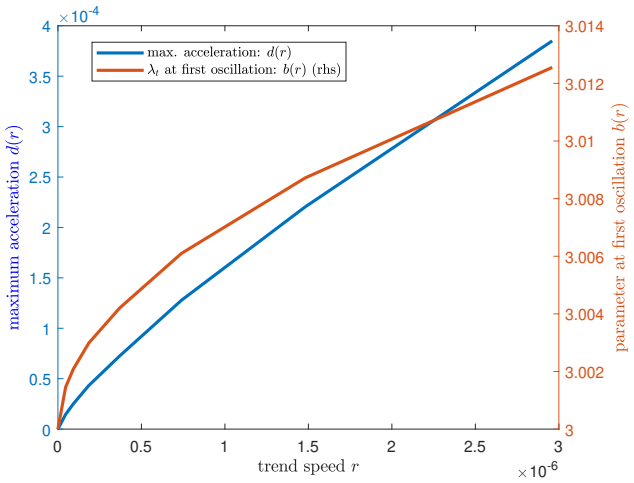

Figure S5: Maximum acceleration $d(r)$ (blue line, left hand vertical axis) and parameter value at first oscillation $b(r)$ (red line, right hand vertical axis) as functions of the rate of environmental change, r.

Delay in bifurcation and onset of Cycling

Figure S6 summarises the abundance time-series in chronological time (1st column, I) and in the re-scaled λ_t time-scale (2nd column, II), for the *very slow* (1st row, *a*), *slow* (2nd row, *b*), *fast* (3rd row, *c*) and *very fast* trend (4th row, *d*) studied in the main text. The 3rd column (III) displays cobweb diagrams of the abundance trajectories in the vicinity of the b-tipping point of the *slow* environmental trend, $\lambda_t = 3.146 = b(r_s)$, for these four different trend speeds. For the *slow* trend, it corresponds to the appearance of the first oscillations (fig.S6bIII). For the *very slow* trend (fig.S6aIII), the time period observed occurs long after the tipping point, $b(r_{vs}) = 3.0009 \ll b(r_s)$: the population follows quasi-2-generation cycles very close to that predicted by the constant environment for $\lambda = 3.144$. For the *fast* trend (fig.S6cIII) it occurs long before, $b(r_s) \ll b(r_f)$: the abundances track the (ghost) "moving equilibrium" (and will do all the way to $t = T$). The different regimes for the same value of the environmentally driven parameter λ, for trends of different speeds, reflect the different regimes for various points along the trajectory for one specific speed r as can be expected from eq. 10.

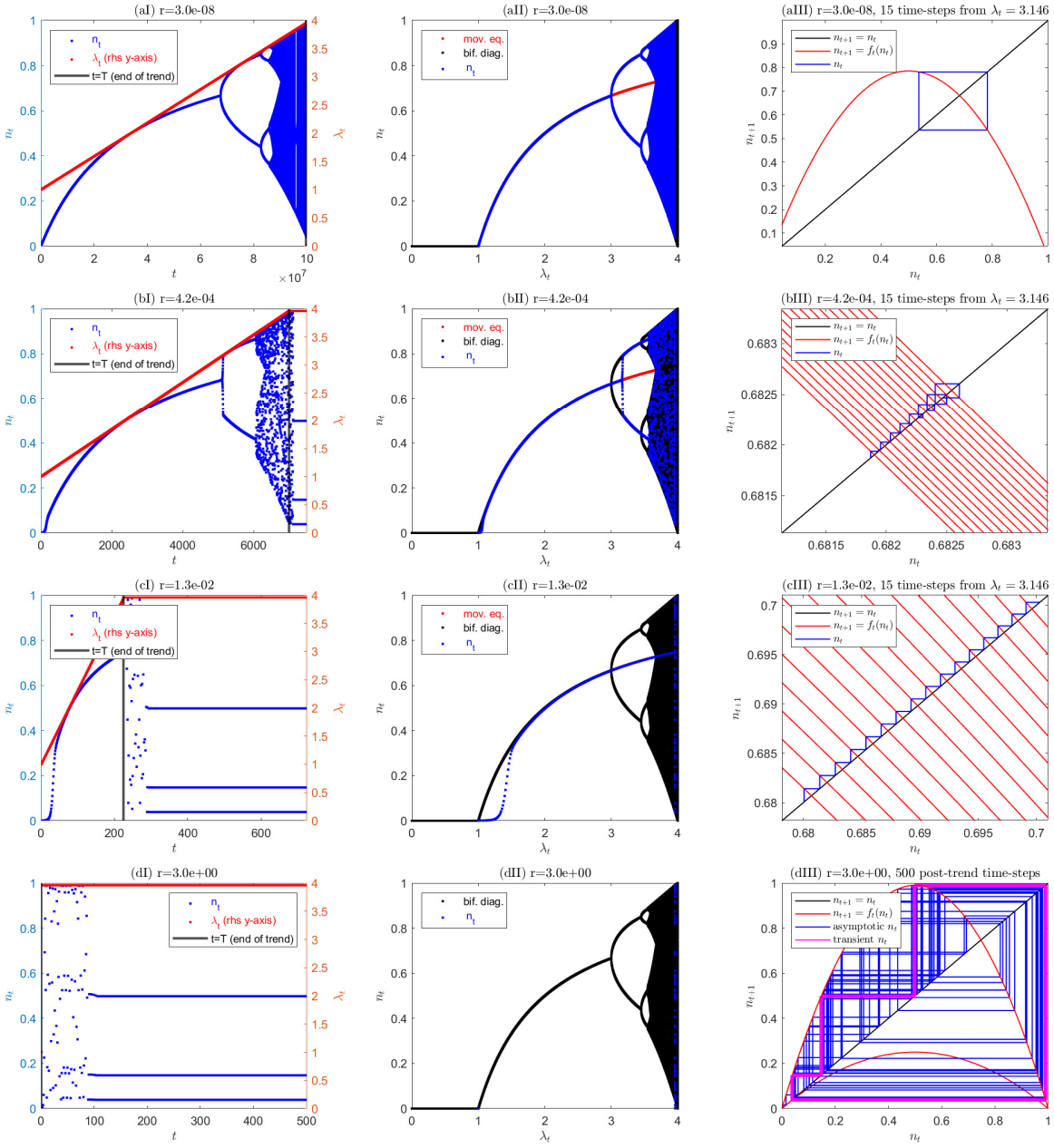

Figure S6: Summarising population dynamics under continuous environmental change corresponding to *very slow* (a, 1st row), *slow* (b, 2nd row), *fast* (c, 3rd row) and *very fast* (d, 4th row) environmental trends (r). (I, 1st column) time-series for abundances (blue) and reproductive rate λ_t (red, secondary axis); (II, 2nd column) superimposition of the abundance time-series (blue) as a function of λ_t overlaying the bifurcation diagram (black) with the moving equilibrium point in red; and (III) cobweb diagrams, with population response curves ($f(n_t)$) in red, 1:1 curve in black and population abundance trajectories in blue

Start of oscillation analysis and r-bifurcation diagrams

In the main text, we display the r-bifurcation diagram for the logistic map and a linear trend in λ_t (fig.7), which shows $b(r)$, the value of λ_t at the first oscillation in abundances (and the duration of the post-trend transient, $D(r)$). We can also perform the same analysis on the chronological time-scale by considering $t_0(r)$, the generation of the first oscillation in abundances (fig.S7).

Figure S7– a loglog plot so that we have $ln(T)$ as linear function of $ln(r)$ – shows that t_o (in blue)

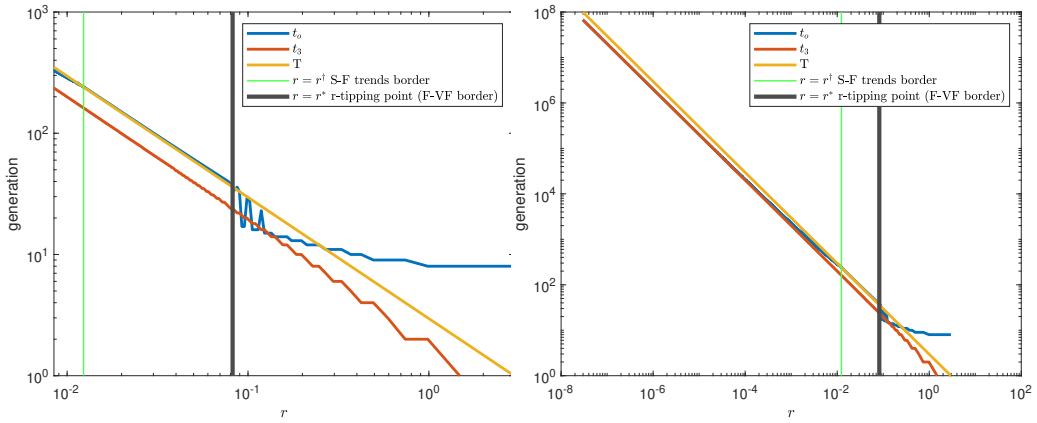

Figure S7: The generation of first oscillation t_o (blue line), the generation t_3 at which $\lambda_{t_3} = 3$ (red line), and the number of generations of the trend T (orange line), for various values of r, on a loglog scale. The 2 figure panels differ only by the range of r displayed. Green and grey vertical lines illustrate borders between qualitatively different rates of environmental change.

is a decreasing function of r, up until the r-tipping point r^*. The r-tipping-point (r^*) segregates monotonic $t_0(r)$ for *fast* trends ($r < r^*$) and non-monotonic $t_0(r)$ for *very fast* trends ($r > r^*$). In the monotonic range, $r^{\dagger}$ segregates the range where $t_0 > T$ (*fast* trends, $r^{\dagger} < r < r^*$) and where $t_3 < t_0 < T$ (*slow* and *very slow* trends, $r < r^{\dagger}$); where t_3 is such that $\lambda_{t_3} = 3$. As the rate of environmental trends slows towards 0 ($r \to 0$), the generation of the first abundance oscillation tends towards the constant framework bifurcation ($t_o(r) \to t_3$). The *very fast* trends range is characterised by r values for which $t_0 < T$, that is, where the first oscillation occurs before the end of the environmental trend; but fig.S7 also shows that we can have $t_0 < t_3$ in that range; that is, oscillations before reaching the cycle range ($\lambda < 3$).

Figure S7 illustrates that on the λ_t time-scale, we have $\lim_{r\to 0} b(r) - 3 = 0$, while on the chronological time-scale $\lim_{r\to 0} t_o(r) - t_3(r) = +\infty$. It can be easier to understand why, by

considering both the time at which the first decline in population size is observed, $t_o(r)$, and the number of generations for which the abundance keeps increasing monotonically having passed the constant environment bifurcation point, $\lambda_{t_3} = 3$, that is $t_o - t_3$, as per fig.S8. It helps to understand why the slower the environmental trend, the longer (in number of generations) the population increases monotonically after having passed $\lambda = 3$, and the (chronological) delay in oscillation $(t_o(r) - t_3(r))$ tends towards ∞ as r tends towards 0. While the projection of this delay onto the alternative time-scale λ_t, $b(r) - 3$, increases with the rate of the environmental trend r (fig.7), the opposite is true on the chronological time-scale (blue on fig.S8). In other words, the slower the environmental trend, the longer (in number of generations) the population increases monotonically after having passed $\lambda = 3$, and the (chronological) delay in oscillation $(t_o(r) - t_3(r))$ tends towards ∞ as r tends towards 0. However, this delay in the time of first oscillation $(t_o - t_3)$ decreases more slowly with r than $T - t_o$ (red on fig.S8): relative to the time spent in the trend past t_3, the proportion corresponding to monotonic increases $\frac{t_o - t_3}{(T - t_o) + (t_o - t_3)}$ increases with r and tends towards 0 as r does. On fig.S8, the border separating the *slow* and *fast* trends ($r^\dagger$) corresponds to a difference in slope of $\frac{ln(t_o - t_3)}{ln(r)}$, caused by the fact that, for *fast* trends, $t_o = T$, so this slope is "forced" at -1. It also corresponds to the point where $T - t_o$ becomes zero (for *fast* trends) and cannot be computed on a log scale (red on fig.S8) Contrary to the *fast* trends, for *very fast* trends we can have $t_o < T$, so that $T - t_o$ can be displayed for some values of r on the loglog plot (in red).

Around the r-tipping point

It is clear from the r-bifurcation diagram (fig.7) that there is regime shift at r^*, segregating a smooth regime, for $r < r^*$, where $b(r)$ decreases monotonically (first as a plateau, then as a strictly decreasing function) from $b(r^*) = \lambda_T$ to the limit $\lim b(r)_{r \to 0} = 3$. In fig.S9, we illustrate this by providing the dynamics of the trendy logistic map for rates of environmental change r in the vicinity of r^*.

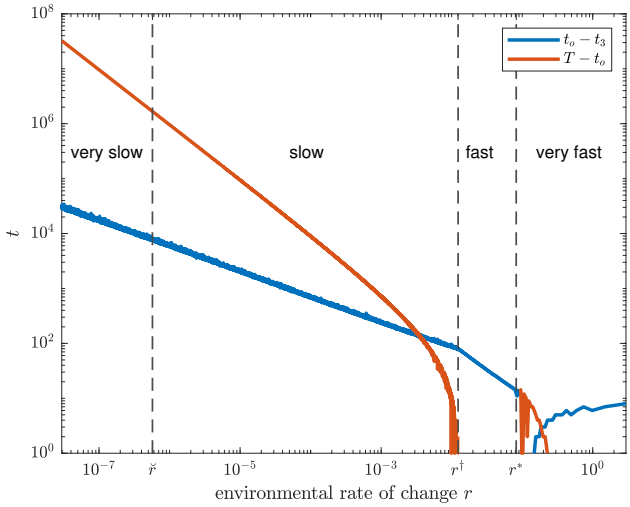

Figure S8: *r-bifurcation diagrams* illustrating quantitative characterisation of four qualitatively different rates of environmental change (*very slow*, *slow*, *fast* and *very fast*; r on the (chronological) delay in oscillations $t_o - t_3$ and the (chronological) duration of the portion of the trend after the first oscillation $T - t_o$, on a log scale

Other period doubling bifurcations

For certain rates of environmental change r, the abundance time series can display a delay in the second period doubling bifurcation (from 2- to 4-generation cycles; fig.S10): abundances keep tracking the 2-generation cycle ghost equilibrium past the constant-environment bifurcation, before abruptly shifting to quasi-4-generation cycles. However, despite the self-similarity of the logistic map, it is possible for a given speed of environmental change (r) to encounter a b-tipping point at one period-doubling bifurcation and not others (as for r_s, see fig.3).

A3 Auto-correlation of the noisy stationary logistic map

For the logistic map in a noisy (but stationary) environment, that is, for example, for

$$\begin{cases} n_{t+1} = \lambda_t n_t (1 - n_t) \\ \lambda_t = max(0, min(\bar{\lambda} + \epsilon_t, 4)) \\ \epsilon_t \sim \mathcal{N}(0, \sigma_e^2) \end{cases} , \tag{22}$$

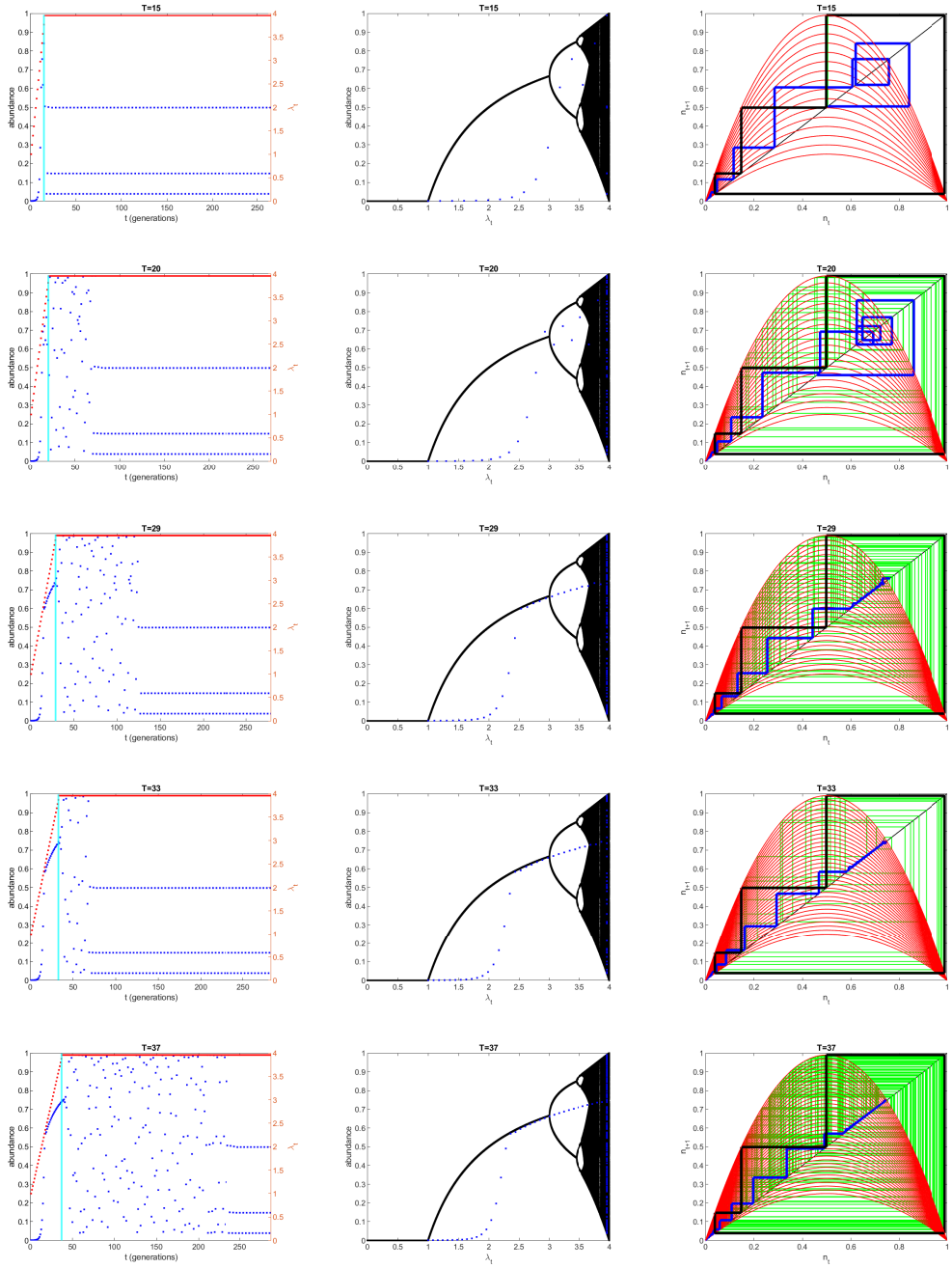

Figure S9: Summarising population dynamics under continuous environmental change for various values of T (rows), on both sides of the r-tipping point r^*, corresponding to $T = 34$. Plots of the abundances over time (left column), the superimposition of the abundance dynamics over the bifurcation diagram (centre column) and the cobweb diagram (right column), where response curves are in red, asymptotic dynamics in black, trend dynamics in blue and post-trend transient dynamics in green

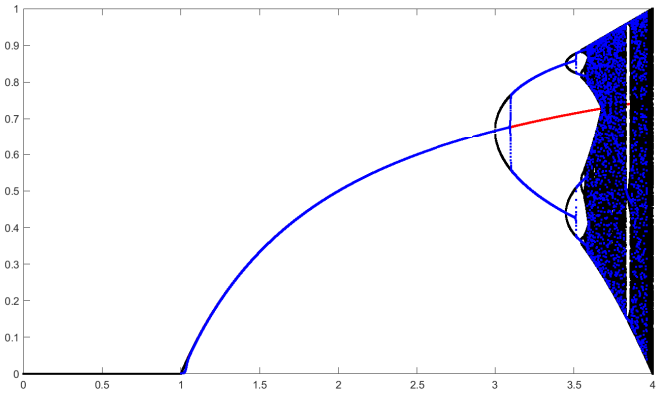

Figure S10: Population size n_t (in blue) given as a function of λ_t for a slow environmental trend ($r \approx 1.5 \times 10^{-4}$ corresponding to $T = 20,000$ generations), superimposed over a classical bifurcation diagram (black), starting at $\lambda_0 = 1.001$ and $n_0 = \hat{n}(\lambda_0)$ and followed by 500 generations at constant $\lambda_T = 3.9605$. The "moving equilibrium" $\hat{n}_t$ is shown in red.

we generate a single time-series for ϵ_t for a standard deviation of $\sigma_e = 0.1$, that we apply to various values of $\bar{\lambda}$ and compute, for each, the corresponding n_t time series (with $n_1 = 0.1$), and its one-generation auto-correlation $\rho(\bar{\lambda}) = \frac{Cov(n_{t+1},n_t)}{var(n_t)}$ (fig.S11). As expected from the deterministic constant environment framework analysis, the autocorrelation is at its lowest in the range $3 < \lambda < 3.44949$ corresponding to 2-generation asymptotic cycles. However, $\rho(\bar{\lambda}) < -0.8$ for $\bar{\lambda} > 2.84$, so that we have quasi-2-generation cycles for $\bar{\lambda}$ in a range corresponding to a stable fixed point equilibrium, corresponding to the overcompensatory transients leading to a stable equilibrium attractor.

A4 A non-linear trend: with no oscillations and constant distance to the moving/ghost equilibrium

For any trend, we never have $\hat{n}_{t+1} = \hat{n}_t = \hat{n}$ as this would imply $\lambda_t = \lambda_{t+1} = \lambda$ a constant environmental parameter (eq.4). From eq.18, we see that similarly, for a linear trend, one can never have $\hat{h}_{t+1} = \hat{h}_t = \hat{h}$. However this is possible for a non-linear trend, and that same equation shows that the speed r_t required for the population abundances to remain at a constant distance to

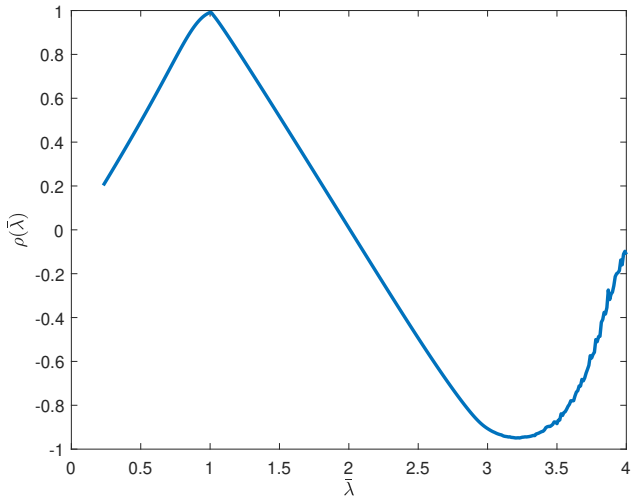

Figure S11: 2-generation auto-correlation $\rho(\bar{\lambda}) = \frac{Cov(n_{t+1},n_t)}{var(n_t)}$ for the noisy stationary logistic map (eq.22). We apply a given $\epsilon_t \sim \mathcal{N}(0, \sigma_e^2)$ time series with $\sigma_e = 0.1$ to a range of mean parameter value $\bar{\lambda}$.

the moving equilibrium, $\hat{h}$, has to increase with time. From eq.14, we can actually build a λ_t time-series that does that, by replacing h_{t+1} and h_t by $\hat{h}$, we get $\hat{h} = (2 - \lambda_t)\hat{h} + \frac{\lambda_t - \lambda_{t+1}}{\lambda_{t+1}\lambda_t}$, which leads to

$$\lambda_{t+1} = \left(\frac{1}{\lambda_t} + \hat{h}(\lambda_t - 1)\right)^{-1} \tag{23}$$

For a given $\hat{h}$, this yields an associated time-series for λ_t that increases exponentially over time (see, for $\hat{h} = -0.001$, the parameter and abundance time series in fig.S12).

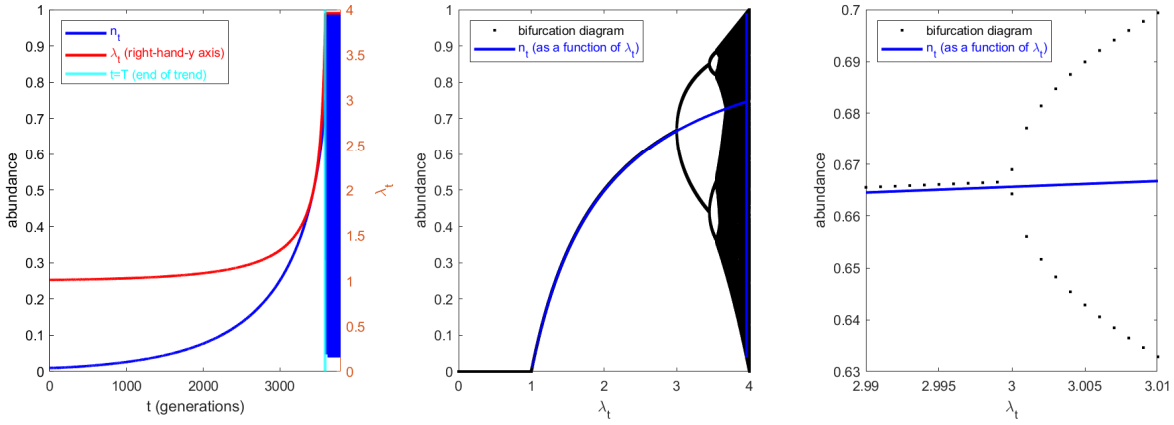

Figure S12: time-series (left), superimposition diagram (centre and right) for λ_t increasing exponentially as per eq.23, with constant distance to ghost attractor: $\hat{h} = -0.001$

A5 The trendy logistic map with a decreasing environmental trend, $r < 0$

Here, we briefly consider a linear trend on the parameter λ of the logistic map (as per the main text) but with negative speeds. That is, the initial and final value of λ_t are reversed: we now have $\lambda_0 = 3.9605$ (4-point cycle) and $\lambda_T = 1.001$ (under-compensatory stable equilibrium attractor). Fig.S13 shows the abundance dynamics both in chronological time (on the left vertical axis) and on the λ_t timescale (on the right axis), for an initial value of $n_0 = 0.1476$, one of the 4 points of the asymptotic cycle corresponding to λ_0. The result corresponds to what our study of $r > 0$ leads us to expect: the dynamics follow the bifurcation diagram for slow trends (the first three rows of the figure), but with a delay: the population encounters chaotic behaviour followed by pseudo-cycles of decreasing period but those occur later (that is, for smaller λ_t values) than the corresponding bifurcation point of the bifurcation diagram. This delay is most noticeable for the bifurcation from 2-generation cycles to a stable equilibrium around $\lambda = 3$: the corresponding end of the pseudo-cycles towards a monotonic decrease in abundances occurs at values of λ_t that decrease with the speed of the trend. Because the delay concerns a transition from cycles to a stable point here, it does not lead to a discontinuity, or b-tipping point, for the abundances. As in the main text, we also note that abundances track the ghost equilibrium corresponding to the stable equilibrium of constant environments but struggle to do so for low values of λ_t: the faster the trend the further from the ghost equilibrium the abundances are as the trend stops. Contrary to the $r > 0$ study, the final value of λ here, $\lambda_T = 1.001$ corresponds to a stable point. The transient post-trend dynamics are much simplified and consist of a monotonic decrease towards $\hat{n}_T \approx 0.001$. For the decreasing λ trend, the $\lambda = 3$ bifurcation is delayed but there is no rate of change that ensure that it is delayed until the end of the trend (no *fast* trends): the $r-$tipping point correspond to the transitions between *slow* trends (delayed bifurcation) and *very fast* trends (no bifurcation, transient dominates). As noted in the main text, the existence of *fast* trends is bifurcation dependent: it depends on the relative rates of change of the moving equilibrium and the

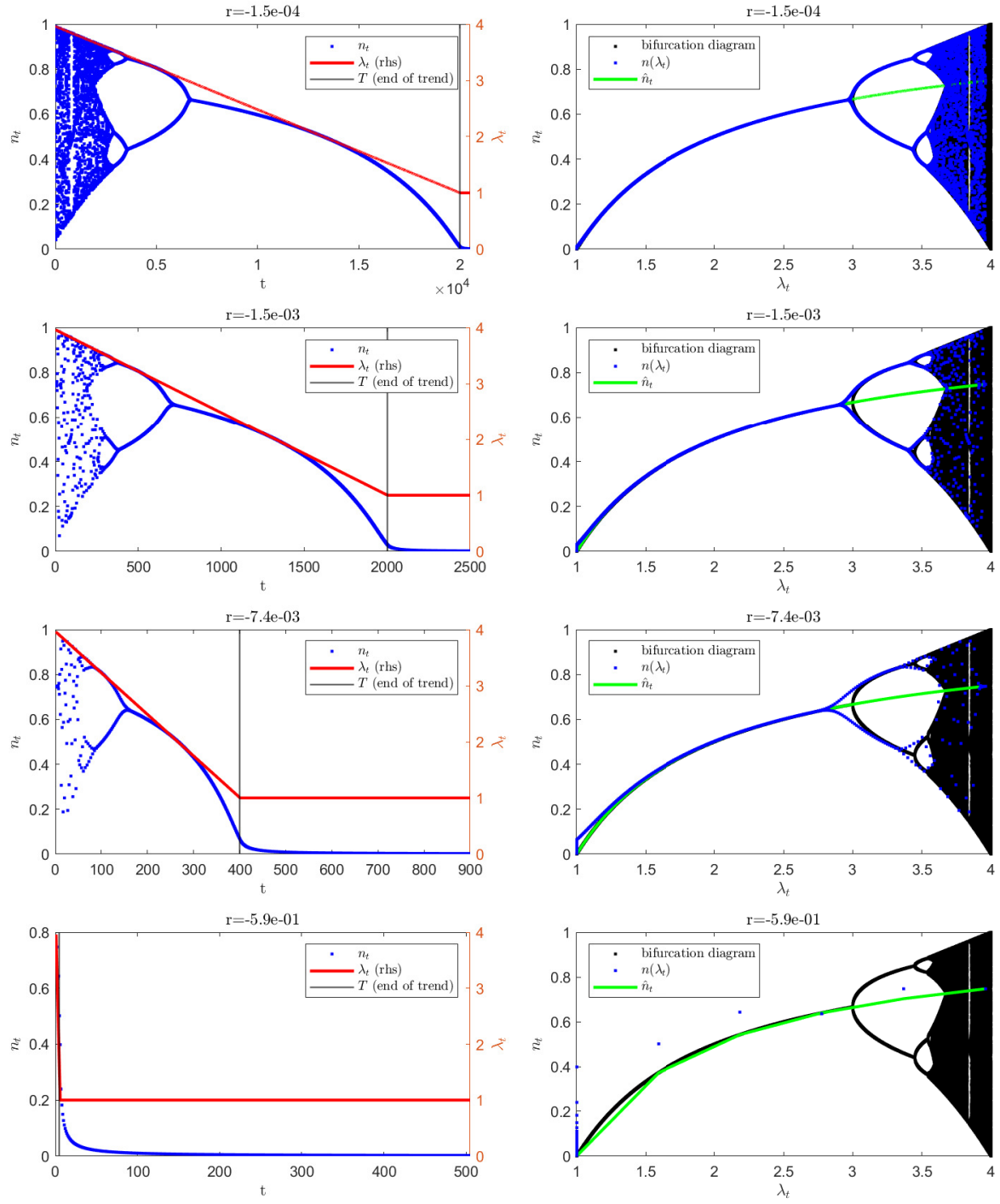

Figure S13: Abundance time-series, n_t (blue points) and λ_t time-series (red, secondary axis) on the left column and – on the right column – superimposition of the abundance time-series (blue points) as a function of λ_t with the bifurcation diagram (black points); for a representative range of values for the rate of environmental change $r < 0$ (different rows) and for $n_0 = 0.1476$

environmental parameter. The difference between *slow* (rows 2 and 3 of fig.S13) and *very slow* (first row) are noticeable via the superimposition diagrams (second column): for the *very slow* trend, the abundances track the moving equilibrium closely enough so that there is no post-trend transient while this transient is noticeable for the *slow* trends (at $\lambda_t \approx 1$ on the panels on the second column and rows 2 and 3).

A6 Transient dynamics of the trendy logistic map

Long Transient Sensitivity to number of steps for a *very fast* trend

Here, we consider what occurs when a sudden environmental change takes more than a single generation, i.e., two or three generations, thereby adding one or two "stepping stones" on the way to the asymptotic cycle. We have seen how sensitive the duration of the transient is to the initial condition of the step change, we therefore expect the same with regards to the number of stepping-stones, as these will directly affect n_T, the initial condition of the last step of the change, which will drive the transient dynamics. Indeed, as we see in the top row of fig.S14, for $T = 2$, the transient is very short (3 generations) while for $T = 3$, illustrated as the bottom row of fig.S14, the transient lasts for 230 generations.

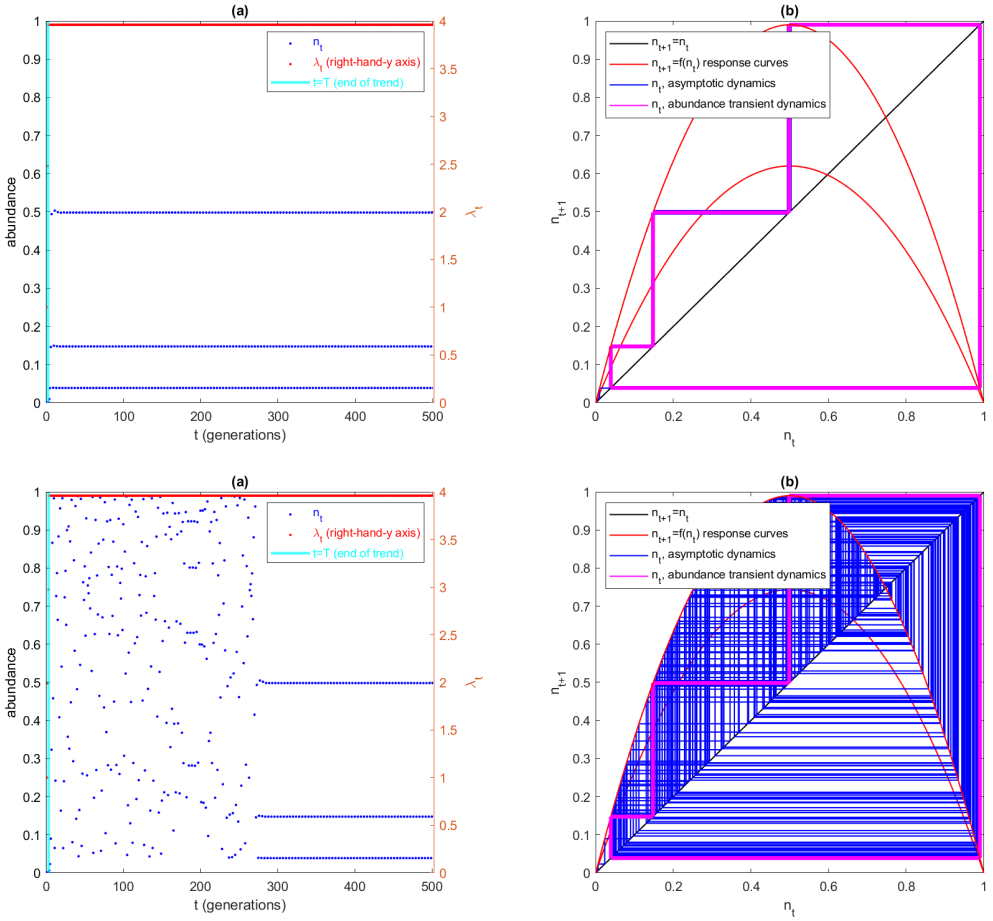

Figure S14: 2-Step ($r \approx 1.45$, $T = 2$, top) and 3-step ($r \approx 0.99$, $T = 3$ bottom) environmental change from $\lambda_0 = 1.001$ and $n_0 = \hat{n}(\lambda_0)$, to $\lambda_T = 3.9605$ followed by 500 generations at that constant environment (λ_T); (a) abundance n_t (blue) and environmental parameter λ_t (red, secondary axis); (b) cobweb diagram: response curves ($f(n_t)$, in red) and the abundance trajectory (n_t, transient phase shown in blue; asymptotic phase shown in magenta). The $n_t = f(n_t)$ line is shown in black.